수의학석사학위논문

아라키돈산에 의한 MT3-MMP 발현의 중간엽 줄기세포 이동 및 창상 치유능 증진 효과

Enhancement effect of arachidonic acid-induced MT3-MMP expression on migration and skin wound healing of mesenchymal stem cell

2018년 2월

서울대학교 대학원

수의학과 수의생명과학 전공

오 상 엽

ABSTRACT

Enhancement effect of arachidonic acid-induced MT3-MMP expression on migration and skin wound healing of mesenchymal stem cell

Sang Yub Oh

Major in Veterinary Biomedical Science

Department of Veterinary Medicine

The Graduate School

Seoul National University

Arachidonic acid (AA) is largely released during injury, but it has not been fully studied yet how AA modulates wound repair with stem cells. Therefore, I investigated skin wound-healing effect of AA-stimulated human umbilical cord blood-derived mesenchymal stem cells (hUCB-MSCs) *in vivo* and its molecular mechanism *in vitro*. I found that transplantation of hUCB-MSCs pre-treated with

AA enhanced wound filling, re-epithelization, and angiogenesis in a mouse skin excisional wound model. AA significantly promoted hUCB-MSCs migration after a 24 h incubation, which was inhibited by the knockdown of G-protein-coupled receptor 40 (GPR40). AA activated mammalian target of rapamycin complex 2 (mTORC2) and Akt^{ser473} through theGPR40/phosphoinositide 3-kinase (PI3K) signaling, which was responsible for the stimulation of an atypical protein kinase C (PKC) isoform, PKCζ. Subsequently, AA stimulated phosphorylation of p38 MAPK and transcription factor Sp1, and induced membrane type 3-matrix metalloproteinase (MT3-MMP)-dependent fibronectin degradation in promoting hUCB-MSCs motility. Finally, the silencing of MT3-MMP in AA-stimulated hUCB-MSCs failed to promote the repair of skin wounds owing to impaired cell motility. In conclusion, AA enhances skin wound healing through induction of hUCB-MSCs motility by MT3-MMP-mediated fibronectin degradation, which relies on GPR40-dependent mTORC2 signaling pathways.

Keywords: arachidonic acid, mesenchymal stem cell, skin wound healing, migration, MT3-MMP

Student Number: 2013-21539

CONTENTS

LIST OF FIGURES

ABBREVIATIONS

AA	Arachidonic acid
BrdU	5-Bromo-2'-deoxyuridine
COL	Collagen
FN	Fibronectin
FBS	Fetal bovine serum
GPR40	G-protein-coupled receptor 40
H&E	Hematoxylin and eosin
hUCB-MSCs	Human umbilical cord blood-derived mesenchymal stem cells
mTORC	Mammalian target of rapamycin complex
MAPK	Mitogen-activated protein kinase
MT3-MMP	Membrane type 3-matrix metalloproteinase
NDGA	Nordihydroguaiaretic acid
PBS	Phosphate-buffered saline
PCR	Polymerase chain reaction
PKC	Protein kinase C
PI3K	Phosphoinositide 3-kinase
PUFA	Polyunsaturated fatty acid

RFU	Relative fluorescence units
ROD	Relative optical density
1-ABT	1-Aminobenzotriazole

INTRODUCTION

Skin wound healing is a dynamic process that involves inflammation, re-epithelization, granulation, vascularization, and tissue remodeling, in which various types of cells migrate into the wound.(Castilho et al., 2013) Many treatment modalities are applicable to improve skin recovery after injury including cytokines/growth factors and cell-based therapies.(Limova. 2010) The use of stem cell therapy has been emphasized as a promising adjunct for delayed wound healing.(Ennis et al., 2013) In this process, the migration of stem cells is an important biological event to exert their beneficial effects at the best place, which effects include paracrine signaling, proliferation, or differentiation and play a key role in cutaneous regeneration.(Castilho et al., 2010; Hocking et al., 2010) Although commonly used approaches to manipulating stem cell behaviors include administration of biochemical cocktails and genetic modifications,(Vaca et al., 2008; Yau et al., 2012) these methods are considered impractical for clinical use owing to

unexpected potential side effects. In this respect, the important factor for the success of stem cell therapy in cutaneous wounds is the capability to regulate stem cell behaviors with predictable methods. Therefore, the development of safe, effective, and practical means to modulate stem cell migration is a priority in the skin wound-healing field.

Many nutrients including lipid metabolites are receiving tremendous attention as emerging key regulators of stem cell behaviors.(Yusuf et al., 2012) Current research on lipids and lipid metabolites has so far revealed a number of signaling pathways and effector molecules involved in cell functions, such as G-protein-coupled receptor 40 (GPR40),(Kim et al., 2009) Src,(Martinez-Orozco et al., 2010) mammalian target of rapamycin (mTOR),(Apte et al., 2013) and matrix metalloproteinases (MMPs).(Kang et al., 2013; Martinez-Orozco et al., 2010) Interestingly, these signaling molecules are also closely related to stem cell behaviors including cytoskeletal reorganization, proliferation, or lineage selection.(Kim et al., 2009; Lee et al., 2014a; Sen et al., 2014) Thus, the specific effects of lipid metabolites on the regulation of stem cell functions are important in stem cell biology as well as stem cell-based therapy, which might differ by cell type, dosage, culture conditions,

and metabolic state. To date, however, despite the fact that arachidonic acid (AA), a representative $\omega-6$ polyunsaturated fatty acid (PUFA), is the second most abundant fatty acid released into a wound site during skin injury(Black et al., 1981; Ziboh et al., 1988) and is implicated in the restoration of various types of tissues including intestine and bone,(Jacobi et al., 2012; Yang et al., 2012) the functional role of AA in stem cell motility is not fully understood. Therefore, the complexity of AA-mediated regulatory networks in stem cell migration is both a challenge and an opportunity for further comprehensive investigations into stem cell-based skin wound therapy.

Mesenchymal stem cells (MSCs) have been shown to ameliorate wound healing in several studies.(Ennis et al., 2013) Human umbilical cord blood-derived mesenchymal stem cells (hUCB-MSCs) are characterized as neonatal stem cells which are abundant, convenient to obtain, capable of multilineage differentiation, and able to self-renew with a high proliferative capacity.(Wang et al., 2009) Because hUCB-MSCs also retain a lower immunogenicity and higher migratory ability, their clinical potential has been assessed with cell-based applications for diseases including chronic skin wounds, colitis, and neurotmesis injuries.(Gartner et al.,

2014; Kim et al., 2013; Ribeiro et al., 2014) Thus, elucidating the role of AA in modulating behaviors of hUCB-MSCs is a promising and practical approach for clinical applications. Therefore, I investigated the role of AA in transplanted hUCB-MSCs for skin wound healing *in vivo* and its molecular mechanism *in vitro*.

MATERIALS AND METHODS

1. Materials

hUCB-MSCs were obtained from the MEDIPOST Co. Ltd (Seoul, Korea). FBS was bought from the Bio Whittaker Inc. (Walkersville, MO, USA). AA, A23187, Bisindolylmaleimide I, BrdU, Indomethacin, LY294002, mitomycin C, NDGA, rapamycin, 1-ABT, and SB203580 were acquired from the Sigma Chemical Company (St. Louis, MO, USA). Phospho-Akt^{ser473}, phospho-Akt^{thr308}, Akt1/2/3, β-Actin, collagen1A, collagen3A, collagen5A, fibronectin, phospho-p38, p38, phospho-JNK, JNK, p-ERK1/2, ERK, lamin A/C, MMP-12, pan-cadherin, PKC α, PKC ε, PKC θ, PKC ζ, PKC, phospho-PKC ζ, and Sp1 antibodies were obtained from the Santa Cruz Biotechnology (Santa Cruz, CA, USA). Phospho-PKC, phospho-mTOR^{ser2481} (mTORC2), phospho-mTOR^{ser2448} (mTORC1), and mTOR were purchased from the Cell Signaling (Beverly, MA, USA). The Akt inhibitor I was acquired from the Calbiochem (La Jolla, Ca, USA).

The CD34, GPR40, phospho-Sp1 and MT3-MMP antibodies were obtained from the Abcam (Cambridge, MA, USA). Mithramycin A was purchased from the Tocris (Bristol, UK). Zymogram gels were bought from the Novex (San Diego, CA, USA). Horseradish peroxidase-conjugated goat anti-mouse and goat anti-rabbit IgG were obtained from the Jackson Immunoresearch (West Grove, PA, USA). All other reagents were used as received and were of the highest purity commercially available.

2. Culture of hUCB-MSCs

Briefly, hUCB-MSCs were cultured without a feeder layer and maintained in α-minimum essential medium (Thermo, MA, USA), 10% FBS, and 1% penicillin and streptomycin in a humidified 5% CO_2 incubator at 37℃. Before experiments, the medium was replaced with the serum-free medium for 24 h. And then the cells were washed twice with PBS and maintained in a serum-free medium including all supplements and indicated agents.

3. Mouse excisional wound splinting model

All animal experiments were performed with the approval of the Institutional Animal Care and Use Committee of Seoul National University (SNU-140123-6) and in accordance with the National Institutes of Health Guidelines for the Care and Use of Laboratory Animals. In addition, 4 authors are Doctors of Veterinary Medicine with licenses granted from the Ministry of Agriculture and Forestry of Republic of Korea. 8 week-old ICR mice (♂) were used and anesthetized using a 1:2 mixture of Xylazine HCl (10 mg/kg, Rompun, Bayer, Germany) and Zoletil (20 mg/kg, Virbac Laboratories, Carros, France) via intra-peritoneal injection prior to all surgery. Mouse cutaneous wounding (two 6-mm wounds on the back) and stem cell implantation were carried out as described previously.(Lee et al., 2014b; Wang et al., 2013) Experimental animals to investigate the functional effect of AA on hUCB-MSCs were separated into four groups (five mice per group); wild type mice received vehicle (group 1) or AA (group 2) without hUCB-MSCs; and mice topically transplanted with hUCB-MSC which were pre-treated with vehicle (group 3) or AA (group 4). Furthermore, to study the role of MT3-MMP in wound healing effect of hUCB-MSCs, mice were divided into four additional groups (five mice per

group) where hUCB-MSCs were pre-treated with 2 μM of BrdU for 24 h before transplantation; mice in two groups were transplanted with hUCB-MSCs/*Nt*siRNA that were pre-treated with vehicle (group 5) or AA (group 6); and mice in the other groups were given hUCB-MSCs/*MT3-MMP*siRNA that were pre-treated with vehicle (group 7) or AA (group 8). I injected 1 x 10^6 hUCB-MSCs in 70 μl PBS containing 50% growth factor- reduced Matrigel (BD Biosciences, NJ, USA) into the dermis at two sites around the wound and also topically spread 0.3 x 10^6 hUCB-MSCs in 30 μl PBS containing the same Matrigel onto the wound bed at day 0 and 5. After that, I put Tegaderm (3M, London, Canada) around the wounds. Images of wounds were made on days 0, 5, and 9 with a digital camera system (D50, Nikon, Tokyo, Japan) at the same camera/subject distance (30 cm). The open areas of wounds at days 5 and 9 were measured using Image J program (NIH, Bethesda, MD, USA) and presented as percentage of the original wound size. The images of inner side of cutaneous wound sites were obtained to evaluate angiogenesis at day 9. The wound tissues were then embedded in O.C.T. compound (Sakura Finetek, Trannce, CA, USA), stored at -70℃, cut into 6-μm-thick frozen sections by using cryosectioning machine, and mounted on Super Frost Plus

slides (Thermo Fisher Scientific, Rockford, IL, USA) for H&E staining and immunohistochemistry. For histomorphometric analysis, the recovered skin regions adjacent to granulation tissue were evaluated at x 100 magnification in H&E stained sections. Hair follicles were counted and the relative hair follicle densities were presented as percentage of the group treated with Vehicle alone or hUCB-MSCs/*Nt*siRNA+Vehicle.

4. Wound healing migration assay

hUCB-MSCs (4 x 10^4cells) were seeded on low 35-mm dishes with silicone inserts (Ibidi, Martinsried, Germany) and cultured until the cells reach around 100% confluence in serum containing medium. After serum starvation for 24 h, the inserts were removed to create a wound field. The cells were incubated additionally for 24 h with 10μM of AA and visualized with an Olympus FluoView™ 300 confocal microscope (Tokyo, Japan) with a x 100 objective.

5. Oris cell migration assay

hUCB-MSCs(3 x 10^2 cells)/100μl were seeded in each well of

Oirs plate (Platypus Technologies, Madison, WI, USA) and incubated for at least 24 h to permit cell adhesion. The cells were cultured until they reach around 70% confluence. After that, inserts were carefully removed and the cells were gently washed with warm PBS. The cells were incubated with 10 μM of AA in serum-free medium for 24 h and then treated with 5 μM of calcein AM for 30 min to stain the cell populations in endpoint assays. By using a microplate reader to measure excitation/emission wavelengths (485/515 nm), migrated cells were quantified.

6. Scratch wound-healing assay

hUCB-MSCs were cultured until 90% confluence in 35-mm dishes and scratched with a sterile cell scraper (Fisher Scientific, Pittsburgh, PA, USA). The border of denuded area was marked with a fine line immediately, and the cells were incubated with 10 μM of AA in serum-free medium. FBS (2%) was treated for positive control. The cell migration was observed with microscope during incubation with a x 100 objective.

7. Western blot analysis

Cell lysates were extracted with lysis buffer (20mM Tris [pH 7.5], 1mM EDTA, 1mM EGTA, 1% Triton X-100, 1mg/mL aprotinin, and 1mM phenylmethylsulfonylfluoride) for 30 min on ice. The lysates were cleared by centrifugation (15,000 rpm at 4° C for 30 min), and then the protein concentration was determined by the Bradford method.(Bradford. 1976) Equal amounts of protein (15 μg) were resolved by 8-12% SDS-PAGE and transferred to PVDF membranes. The membranes were blocked with TBST solution (10mM Tris-HCl [pH 7.6], 150mM NaCl, and 0.05% Tween-20) containing 5% skim milk for 1 h, and incubated with appropriate primary antibodies at 4℃ for overnight. The membrane was then washed and detected with a horseradish peroxidase-conjugated secondary antibody. The membrane was visualized by enhanced chemiluminescence (Amersham Pharmacia Biotech Inc., Buckinghamshire, UK).

8. Subcellular fractionation

Harvested cells were mixed with buffer 1 (250mM sucrose, 50mM

Tris-HCl, 5mM $MgCl_2$) containing protease inhibitor cocktail (PIERCE, Rockford, IL, USA), incubated on an end-over-end shaker for 10 min, and centrifuged at 1000 x g for 10 min. The supernatants containing cytosolic proteins were transferred to iced tubes. The pellets were lysed with buffer 2 (1M sucrose, 50mM Tris-HCl, 5mM $MgCl_2$) containing protease inhibitor cocktail for 30 min and were centrifuged at 6000 x g for 10 min. The supernatants with membrane proteins were transferred to new iced tubes. The remaining pellets were suspended in buffer 3 (20mM Tris-HCl, 0.4M NaCl, 15% glycerol, 1.5% Triton X-100) containing protease inhibitor cocktail and incubated on an end-over-end shaker for 10 min. After centrifugation at 6800 x g for 10 min, the supernatants containing nuclear proteins were collected.

9. Trichloroethanoic acid precipitation

Filtered culture supernatants were mixed with 100% trichloroethanoic acid(w/v) to a final concentration of 30% (w/v) and were incubated overnight at 4℃. Samples were centrifuged at 10,000 x g for 20 min, and then pellets were washed with cold acetone before air-drying. The protein pellets were dissolved by

the same volume of sample loading buffer (40 μl) and subjected to SDS-PAGE.

10. Confocal microscopy

Either frozen sections of the wounds or cultured hUCB-MSCs were fixed with 4% paraformaldehyde in PBS for 10 min, permeabilized with 0.2% Triton X-100 in PBS for 5 min, and blocked with 5% normal goat serum in PBS for 30 min at room temperature. And then the samples were incubated with appropriate primary antibodies for overnight at 4℃. After washing 3 times with PBS, the samples were stained with Alexa 488-conjugated goat anti-mouse/rabbit IgM, phalloidin, or BrdU in PBS containing 1% (v/v) BSA. Also the samples were counterstained with PI at the same time, followed by 3 times of washing for 10 min with PBS. The samples were visualized with an Olympus FluoView 300 confocal microscope with x 100-400 objective.

11. Measurement of calcium influx

Changes in $[Ca^{2+}]_i$ were measured using Fluo-3-AM (Invitrogen

Co., Carlsbad, CA, USA). Cells in confocal 35 mm-diameter coverglass bottom dishes were washed with a Bath solution (140mM NaCl, 5mM KCl, 1mM $CaCl_2$, 0.5mM $MgCl_2$, 10mM glucose, 5.5mM HEPES, pH 7.4), incubated in a Bath solution containing 2mM Fluo-3-AM for 40 min, rinsed, and scanned every second with confocal microscope (Fluoview 300, Olympus, Hamburg, Germany) at excitation/emission wavelengths of 488/515 nm. A23187, a calcium ionophore, was used as a positive control. All analyses of $[Ca^{2+}]_i$ were processed in a single cell, and the results were expressed as the relative fluorescent intensity (RFI).

12. RNA isolation and real-time PCR

By using the RNeasy Plus Mini Kit (Quiagen, Valencia, CA, USA), total RNA was obtained from hUCB-MSCs. RNA was used for reverse transcription to synthesize cDNA using a Maxime RT premix kit of RNA (iNtRON Biotechnology, Sungnam, Korea). According to the manufacturer's instructions with minor modifications as previously described,(Yun et al., 2014a) real-time quantification of MMP isotypes was carried out with a QuantiMix SYBR Kit (PhileKorea Technology, Daejeon, Korea) using a Rotor-

Gene 6000 real time thermal cycling system (Corbett Research, New South Wales, Australia). GAPDH was used as an endogenous control. The primers used in the present study are described in Table 1 or in my previous report.(Yun et al., 2014b)

Table 1. Primers used for polymerase chain reaction.

Gene	Identification	Primer sequence, 5' → 3'
Runx2	Sense	TGGTTAATCTCCGCAGGTCAC
	Antisense	ACTGTGCTGAAGAGGCTGTTTG
Osteopontin	Sense	GCCGAGGTGATAGTGTGGTT
	Antisense	AACGGGGATGGCCTTGTATG
PPARγ	Sense	ACCATGGTGGGTTCTCTCTG
	Antisense	TCAAAGGAGTGGGAGTGGTC
FABP4	Sense	CGTGGAAGTGACGCCTTTCATG
	Antisense	ACTGGGCCAGGAATTTGACGAA
Sox9	Sense	AGTCGGTGAAGAACGGGCA
	Antisense	AAGTCGATAGGGGGCTGTCTG
Col2a1	Sense	CAACACTGCCAACGTCCAGA
	Antisense	CTGCTTCGTCCAGATAGGCA
VE-Cadherin	Sense	ATGACAATGCCCCGGAGTTT
	Antisense	TGTTGGCCGTGTTATCGTGA

PECAM1	Sense	GGACCCTCGTGGATGTTGTA
	Antisense	CTGCTCGGTTCTCTCTGTGA
Cox-1	Sense	TGTGTTGATGCACTACCCCC
	Antisense	TTGTGCTCACGTAGCCAGAG
Cox-2	Sense	GGCCATGGGGTGGACTTAAA
	Antisense	CCCCACAGCAAACCGTAGAT
ALOX5	Sense	AAGGGCGTGGTGACCATTGAG
	Antisense	CGAGGTTCTTGCGGAATCGG
ALOX12	Sense	TCTCTATGCCCATGATGCTTTACG
	Antisense	GGTGAGGAAATGGCAGAGTTGAC
ALOX15	Sense	ACACTTGATGGCTGAGGTCATTG
	Antisense	GGTCGAAAATTCCCATGTCAGAG
CYP4A11/22	Sense	CTTCTGCTGCTGATCAAGGC
	Antisense	AGGACAGGCACTTGGGAATG
CYP2J2	Sense	CTGCGATGGGCTCTGCTTTA
	Antisense	TGCACCTCATGGATGACAGC

13. Small-interfering RNA transfection

hUCB-MSCs were grown until 70% confluence. The cells were transfected with *MT3-MMP* (25nM), *GPR40* (100nM), or *non-*

targeting (*Nt*) siRNA (25 or 100nM) (Dharmacon, Lafayette, CO, USA) using HiPerFect (QIAGEN, Valencia, CA, USA) for 24 h according to the manufacturer's instructions. The sequences of *GPR40*siRNA were 5'-CGCUCAACGUCCUGGCCAU-3', 5'-GUGACCGGUUACUUGGGAA-3', and their complement. The sequences of *MT3-MMP*siRNA were 5'-ACAGGGUGAUGGAUGGAUA-3', 5'-CAAUGUGGAGGUUUGGUUA-3', and their complement. The sequences of *Nt*siRNA were 5'-UAGCGACUAAACACAUCAA-3' and its complement.

14. Cell counting

hUCB-MSCs (4 x 10^5 cells) were seeded per wells and cultured until they reach around 70% confluence. After serum starvation for 24 h, cells were incubated with 10 μM of AA up to 48 h, and the number of cells was counted at different time points using a hemocytometer.

15. [^{3}H]-thymidine incorporation assay

hUCB-MSCs were synchronized by culture in serum-free media for 24 h and then incubated with 10 μM of AA for 0 - 48 h. After the incubation period, 1 μCi of [methyl-^{3}H]-thymidine (specific activity: 74 GBq/mmol, 2.0 Ci/mmol; Amersham Biosciences, Buckinghamshire, UK) was added to the cultures for 1 h at 37℃. Cellular [^{3}H]-thymidine uptake was quantified by liquid scintillation counting (Wallac, Turku, Finland) in harvested cellular material. All values were converted from absolute counts to percentages of control.

16. Gelatin zymography

Whole cell lysate samples were resolved under non-reducing conditions on 10% SDS-PAGE gels embedded with 1 mg/ml gelatin. Gels were rinsed for 30 min each in buffer 1 (50mM Tris, 2.5% Triton X-100, pH 7.5) and buffer 2 (50mM Tris, 5mM $CaCl_2$, 1 μM $ZnCl_2$, 2.5% Triton X-100, pH 7.5), and then incubated in buffer 3 (50mM Tris, 5mM $CaCl_2$, 1 μM $ZnCl_2$, pH 7.5) for 12 h at 37℃. The gels were stained with Coomassie Blue, and areas of gelatinolytic

were visualized as transparent bands.

17. MTT assay

Cell viability was assessed by using the conversion of 3-(4,5-dimethyl thiazolyl-2)-2,5-diphenyl tetrazolium bromide (MTT) to formazan via mitochondrial oxidation. A total of 10 μl MTT solution was added to each well for 2 h. The mediums were then removed and cells were incubated with 150 μL of DMSO for 30 min. Absorbance at 570 nm was recorded using a spectrophotometer.

18. Statistical analysis

All results are expressed as mean value ± standard errors (SE). All experiments were analyzed by ANOVA, and some experiments were evaluated by comparing treatment means to the control using the Bonferroni-Dunn test. Difference at $P< 0.05$ was considered statistically significant.

RESULTS

1. AA amplified both skin wound healing capacity and migration of hUCB-MSCs.

In order to evaluate the cutaneous wound healing effect of hUCB-MSCs and AA, I grossly assessed wound closure and neovascularization in a mouse skin excisional wound model. The group transplanted with AA-stimulated hUCB-MSCs showed the fastest wound closing (Figure 1A) and neovascularization (Figure 1B), while the control group treated with vehicle alone exhibited the slowest wound healing and few vessels. Intriguingly, addition of hUCB-MSCs+vehicle has stimulatory effect on wound closing and neovascularization, compared with the vehicle alone. However, my data revealed there was no statistical difference between AA alone and vehicle in angiogenesis, indicating AA alone did not show a significant enhancing effect on angiogenesis despite of its promoting

effect on skin wound closure. This means that the wound healing induced by direct treatment of AA on wound bed is an independent mechanism of the angiogenesis that was initiated from hUCB-MSCs activated by AA. Thus, stem cells primed by AA appear to have specific modes of action that differ from ectopic application of AA in promoting the skin wound healing. Histological evaluation of skin wounds by H&E staining showed that the granulation tissue of wounds treated with AA or hUCB-MSCs did not make intimate contact with the surrounding tissue. In contrast, transplantation of hUCB-MSCs pre-treated with AA induced intimate contact of granulation and wound maturation (Figure 1C). The result of histomorphometric analysis revealed that the group transplanted with hUCB-MSCs pre-treated with AA has more hair follicle density in recovered skin tissue (Figure 1D).

For wound restoration, stem cell migration is a prerequisite for recruitment to the wound site.(Kwon et al., 2013) Thus, I investigated the effect of AA on hUCB-MSCs migration by treatment with various concentrations of AA for 24 h. AA statistically enhanced the cell migration at 5 and 10 μM, but not at higher concentrations (Figure 2A). In addition, treatment with 10 μM of AA for various time periods promoted hUCB-MSCs migration

in a time-dependent manner (Figure 2C). The same results were visually confirmed with scratch wound-healing assay (Figure 2B, D). To determine how much the AA-enhanced cell migration solely accounts for covering the mechanically denuded area in the migration assays, proliferation of the cells was evaluated with Mitomycin C, a cell cycle arresting compound. The cell proliferation was found to increase much less compared to the cell migration (Figure 3A). Although the little effect of AA on hUCB-MSCs proliferation was seen in the result of cell counting (Figure 3B), the results after the [^{3}H]-thymidine incorporation of hUCB-MSCs revealed that AA did not show any stimulatory effect on the cell proliferation (Figure 3C). I have performed additional experiments to check whether AA induces the differentiation of hUCB-MSCs *in vitro*. As shown in Figure 4, however, the mRNA expression of differentiation markers for osteoblast (*Runx2, Osteopontin*), adipocyte (*PPARγ, FABP4*), chondrocyte (*Sox9, Col2a1*), and endothelial cell (*VE-Cadherin, PECAM1*) was not significantly regulated by 10 μM of AA treatment for 9 days, suggesting that 10 μM of AA treatment for 9 days seems not to be enough to initiate the differentiation of hUCB-MSCs. Importantly, AA did not have any significant effect on the expression of *COX-1*, *COX-2*, *ALOX5*,

ALOX12, *ALOX15*, *CYP4A11/22*, and *CYP2J2*, which are major enzymes involved in AA metabolism (Figure 5A). Moreover, the cell migration induced by AA was not regulated by pre-treatment with non-selective inhibitors for COX (indomethacin), LOX (NDGA), and CYP (1-ABT) (Figure 5B), suggesting that hUCB-MSCs migration is truly attributed by AA itself, but not by AA metabolites. Interestingly, the AA-induced cell migration was abolished by transfection with small-interfering RNA (siRNA) for a membrane receptor for ω-6 PUFAs, GPR40, in an *in vitro* wound-healing migration assay (Figure 6A) and in an Oris cell migration assay (Figure 6B), indicating the involvement of GPR40 in AA-promoted hUCB-MSCs motility.

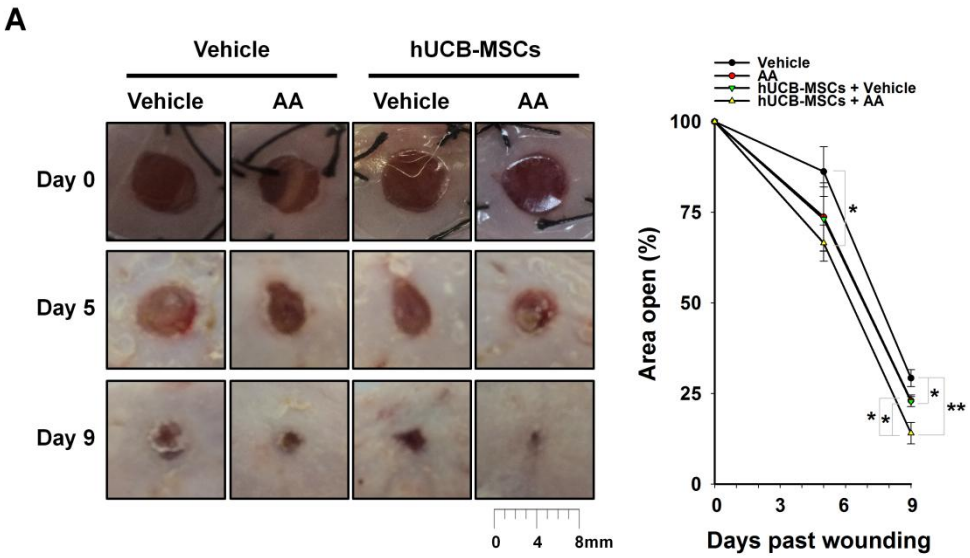
A
Vehicle
hUCB-MSCs
Vehicle
AA
Vehicle
AA
Day 0
Day 5
Day 9
0 4 8mm
Vehicle
AA
hUCB-MSCs + Vehicle
hUCB-MSCs + AA
Area open (%)
100
75
50
25
0
0 3 6 9
Days past wounding
*
*
**
**

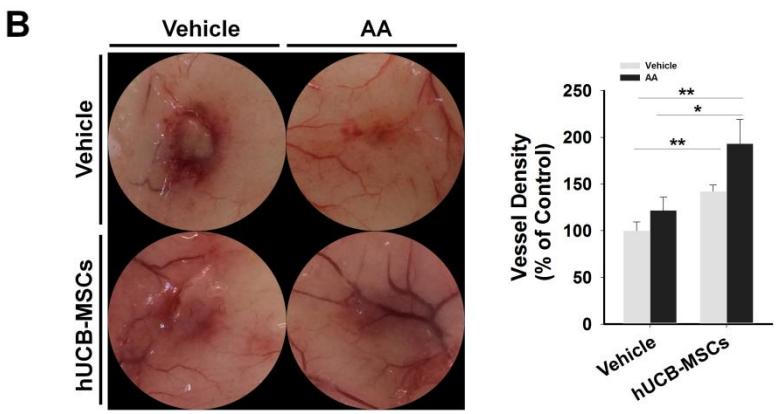
B
Vehicle
AA
Vehicle
hUCB-MSCs
Vehicle
AA
Vessel Density
(% of Control)
250
200
150
100
50
0
**
*
**
Vehicle
hUCB-MSCs

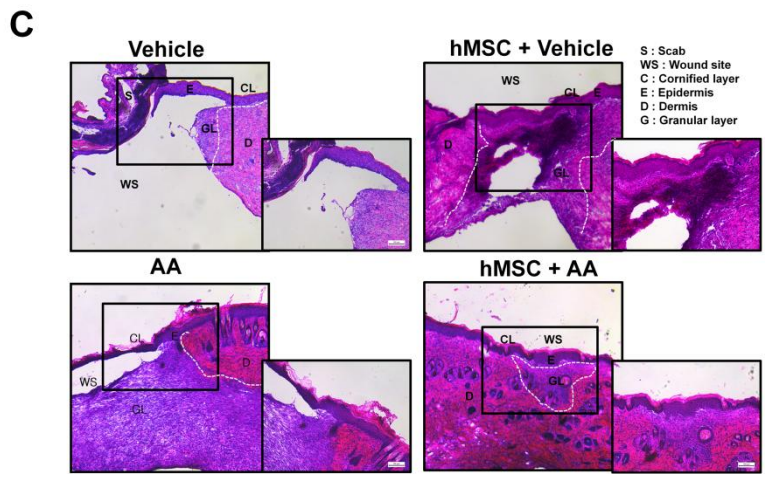
C
Vehicle
hMSC + Vehicle
AA
hMSC + AA
S : Scab
WS : Wound site
C : Cornified layer
E : Epidermis
D : Dermis
G : Granular layer
S
C
E
CL
GL
D
WS

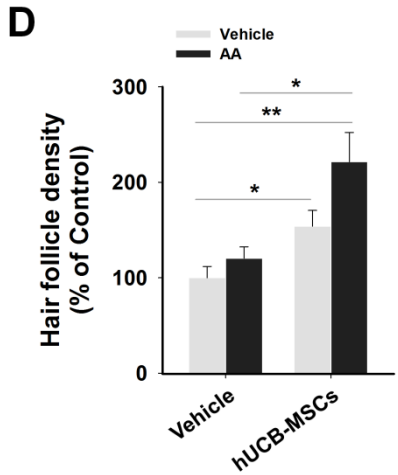

Figure 1. AA enhances skin wound healing effect of hUCB-MSCs. Two 6-mm wounds were made on the back of each ICR mouse, where we treated vehicle, AA, hUCB-MSCs + vehicle, and hUCB-MSCs + AA respectively by topical application and intradermal injection. **(A)** Representative images of mouse cutaneous wounds on postoperative days are shown. Open wound areas relative to the original wound size were quantified with Image J program. **(B)** Representative images of neovasculature in wounds at day 9. Vessel densities relative to the group treated with Vehicle alone were quantified by using Image J program. **(C)** Representative H&E sections of wound tissues at day 9 are shown. **(D)** Hair follicle densities relative to the group treated with Vehicle alone were quantified. (A-D) n = 5. Error bars represent the mean ± SE. $*P < 0.05$, $**P < 0.01$. Scale bars = 100 μm

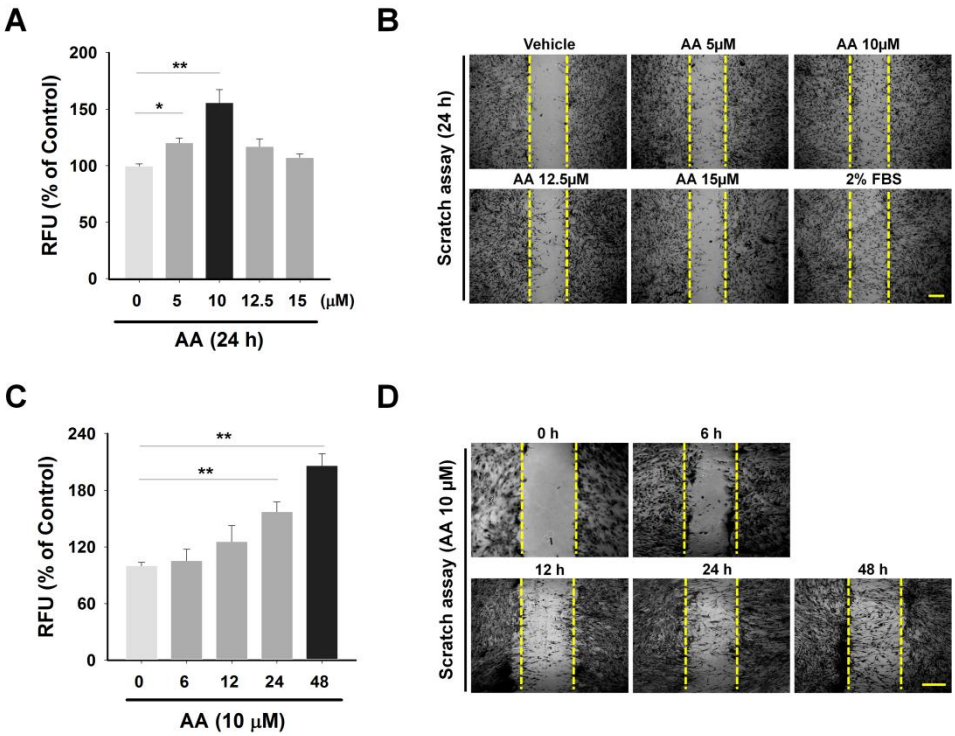

Figure 2. Effect of AA on hUCB-MSCs migration. (A, C) Dose and time responses of hUCB-MSCs treated with AA in Oris cell migration assay are shown. Cells were incubated with different doses of AA (5 – 15 μM) for 24 h and with 10 μM of AA for different time periods (0 – 48 h) respectively. **(B, D)** The dose and time responses to AA are also shown in scratch assay. Cells were treated with AA in the same manner as used in Figure 2A and C. 2 % FBS was added for positive control. (A-D) n = 3. Data represent means ± SE. $*P < 0.05$, $**P < 0.01$, $***P < 0.001$. Scale bars = 100 μm

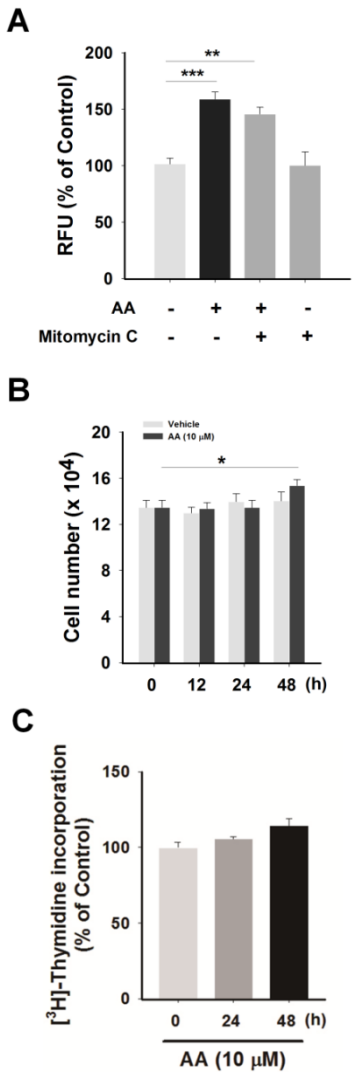

Figure 3. AA has no stimulatory effect on hUCB-MSCs proliferation. (A) Cells were pre-treated with the Mitomycin C (1 μg/ml) for 30 min, stimulated with 10 μM of AA for 24 h, and then assessed with Oris cell migration assay. **(B)** Cells were incubated with 10 μM of AA for 0–48 h and analyzed for their proliferation by cell counting. **(C)** hUCB-MSCs were synchronized by serum starvation for 24 h and then treated with 10 μM of AA for 48h. [^{3}H]-thymidine incorporation was determined. (A) n = 4. (B) n = 6. (C) n = 3. (A-C) Data represent means ± SE. *P< 0.05, **P< 0.01, ***P< 0.001.

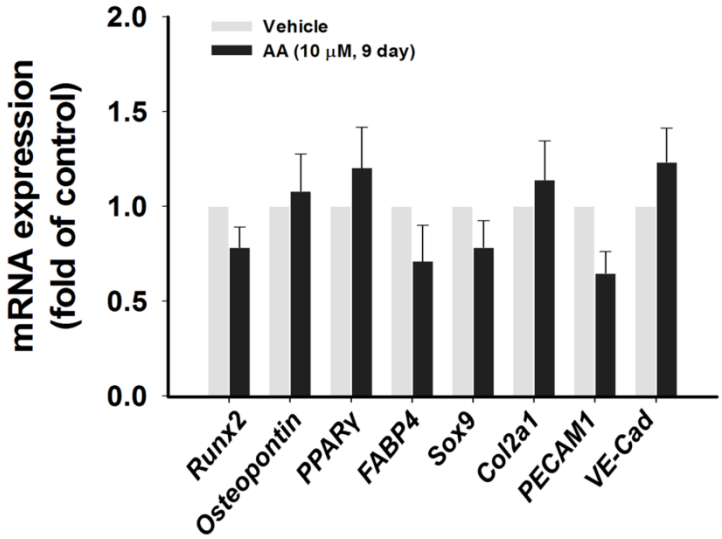

Figure 4. The role of AA in differentiation of hUCB-MSCs. hUCB-MSCs were incubated with 10 μM of AA for 9days. The mRNA expression of differentiation makers for osteoblast (*Runx2*, *Osteopontin*), adipocyte (*PPARγ*, *FABP4*), chondrocyte (*Sox9*, *Col2a1*), and endothelial cell (*VE-Cadherin*, *PECAM1*) was assessed by using real-time PCR as described in Materials and Methods. n = 3. Data represent means ± SE.

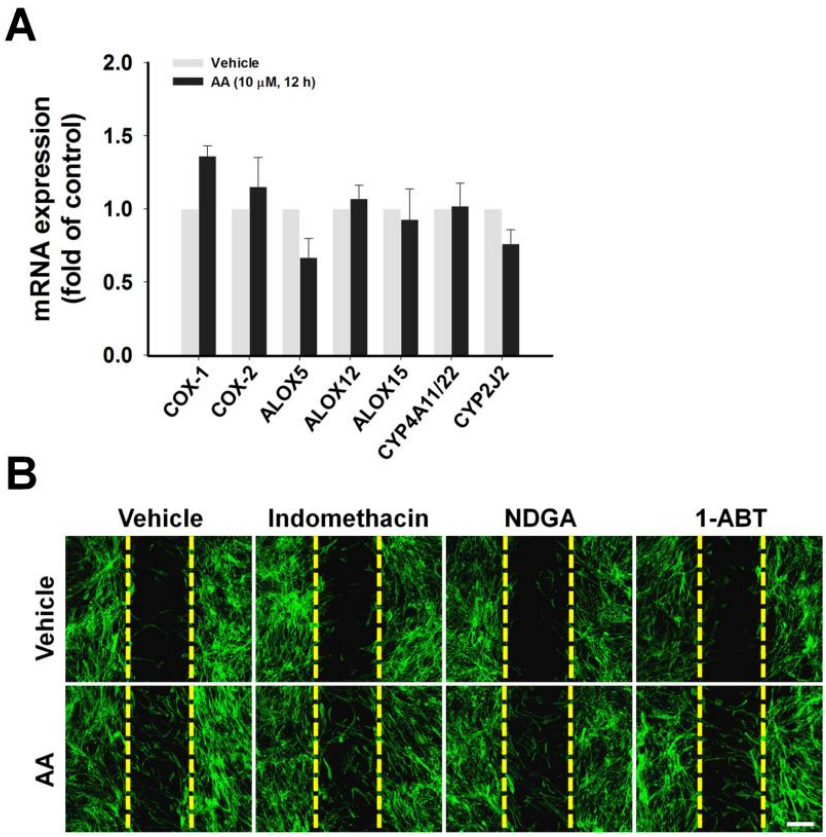

Figure 5. AA metabolism does not regulate the motility of hUCB-MSCs. (A) hUCB-MSCs were treated with 10 μM of AA for 12 h. The mRNA expression of *COX-1, COX-2, ALOX5, ALOX12, ALOX15, CYP4A11/22*, and *CYP2J2* was measured by using real-time PCR as described in Materials and Methods. **(B)** hUCB-MSCs were pre-treated with indomethacin (10μM), NDGA (10μM), and 1-ABT (10μM) for 30 min prior to AA (10 μM) exposure for 24 h. Wound-healing assay was performed. (A, B) n=3. Data represent the means ± SE. Scale bar = 200 μm

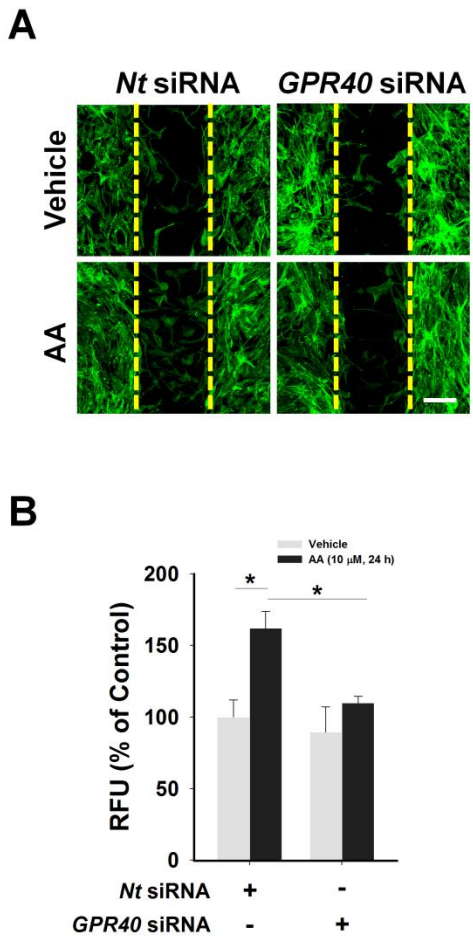

Figure 6. Involvement of GPR40 in AA-promoted hUCB-MSCs migration. 24 h after transfection with *GPR40* specific siRNA (100 nM), cells were incubated with 10 μM of AA for 24 h. And then their motility was assessed with **(A)** wound healing assay and **(B)** Oris cell migration assay. (A, B) n = 3. Data represent means ± SE. *$P<$ 0.05. Scale bars = 100 μm

2. AA activates mTOR^{ser2481}, Akt^{ser473}, and PKCζ through GPR40/PI3K signaling.

I further examined whether the GPR40/PI3K/mTOR pathway is involved in promoting the motility of hUCB-MSCs. The phosphorylation of mTOR^{ser2481} (mTORC2) induced by AA peaked at 30 min and mTOR^{ser2448} (mTORC1) did at 60 min (Figure 7A). I focused on the early-activated mTORC2 which are present at upstream signaling network compared to mTORC1.(Tanaka et al., 2011) The AA-induced increase in phosphorylation of mTORC2 was significantly abrogated by transfection with *GPR40*siRNA (Figure 7B) and by pre-treatment with PI3K inhibitor, LY294002 (Figure 7C). I then assessed phosphorylation of Akt closely associated with mTOR signaling. The phosphorylation level of Akt^{ser473} increased until 60 min in contrast to stationary Akt^{thr308} (Figure 8A). In addition, the phosphorylation of Akt^{ser473} was blocked by prolonged rapamycin pre-treatment which is able to inhibit mTORC2 (Figure 8B).(Sarbassov et al., 2006) I also found that AA-induced cell motility was inhibited by LY294002, rapamycin, and Akt inhibitor I in an *in vitro* wound-healing

migration assay (Figure 8C) and in an Oris cell migration assay (Figure 8D).

I further checked the involvement of PKC in signaling pathway induced by AA. The phosphorylation of PKC was detected from 60 to 120 min (Figure 9A). Among conventional (PKC α), novel (PKC θ, ε), and atypical (PKC ζ) PKC isotypes, only atypical PKC ζ translocated from the cytosol to the membrane in response to AA treatment (Figure 9B). The membrane translocation was visually confirmed by immunofluorescence staining in AA-treated hUCB-MSCs (Figure 9C). Because atypical PKC do not need calcium for activation, there was no calcium influx in AA-stimulated hUCB-MSCs (Figure 9D). In addition, the PKC ζ activation was blocked by pre-treatment with Akt inhibitor I (Figure 10A) and rapamycin (Figure 10B). I also found that AA-induced cell motility was inhibited by PKC inhibitor, Bisindolylmaleimide I in an *in vitro* wound-healing migration assay (Figure 10C) and in an Oris cell migration assay (Figure 10D).

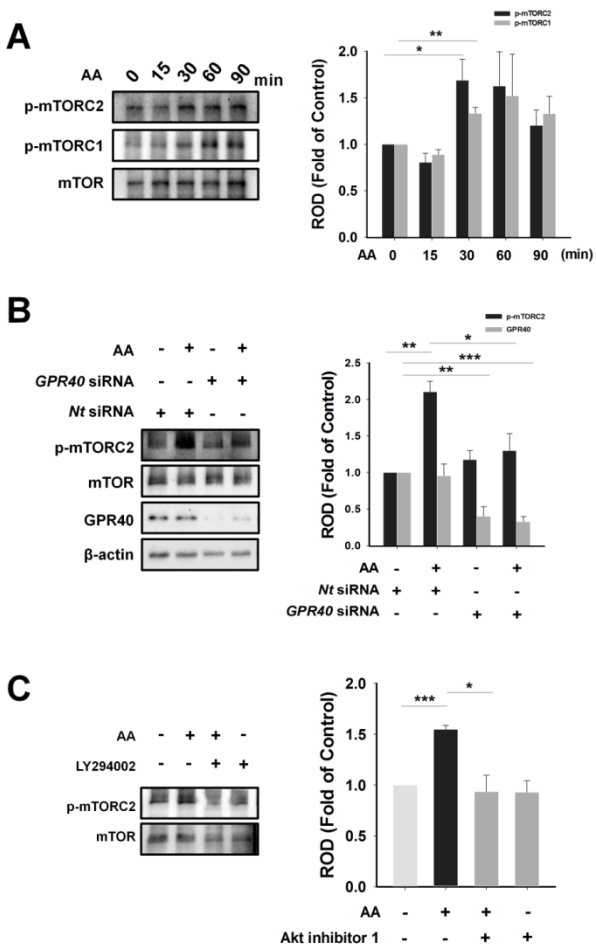

Figure 7. AA activates mTOR through GPR40/PI3K signaling. (A) hUCB-MSCs were incubated with 10 μM of AA for various time periods (0-90 min). Total proteins were extracted and blotted with phosphor-mTOR^{ser2448}, phosphor-mTOR^{ser2441} or mTOR. **(B)** Cells transfection with *GPR40*siRNA (100 nM) were incubated with 10 μM of AA for 30 min and then the levels of phosphor-mTOR^{ser2441}, mTOR, GPR40, and β-actin were examined by Western blotting with total cell lysates. **(C)** Cells pre-treated with 10 μM of LY294002 for 30 min were incubated with 10 μM of AA for 30 min. phosphor-mTOR^{ser2441} and mTOR were detected by Western blotting. (A-C) n = 3. Data represent means ± SE. $*P < 0.05$, $**P < 0.01$, $***P < 0.001$.

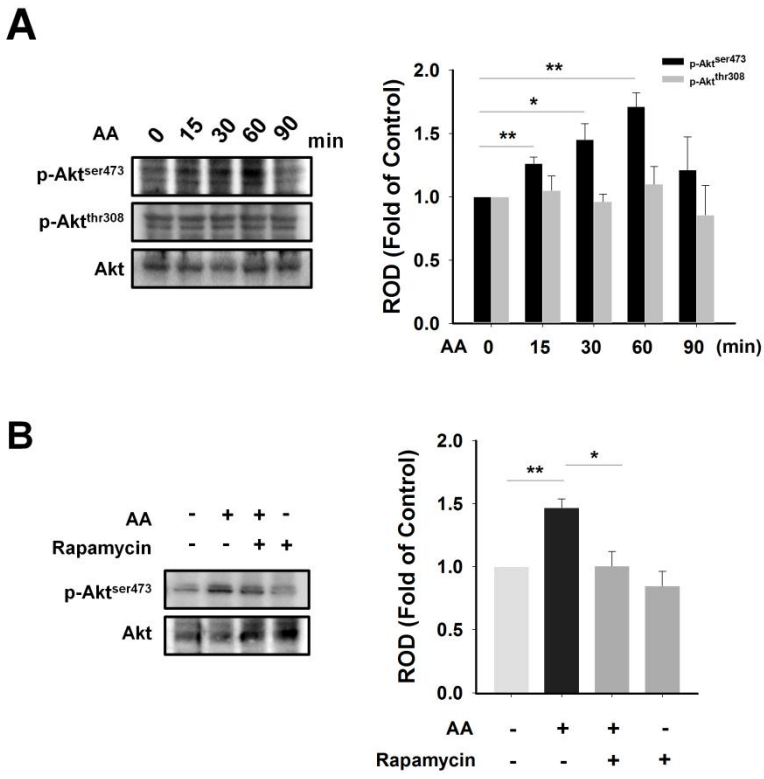
A
AA 0 15 30 60 90 min
p-Akt^ser473
p-Akt^thr308
Akt
ROD (Fold of Control)
2.0
1.5
1.0
0.5
0.0
**
*
**
p-Akt^ser473
p-Akt^thr308
AA 0 15 30 60 90 (min)
B
AA - + + -
Rapamycin - - + +
p-Akt^ser473
Akt
ROD (Fold of Control)
2.0
1.5
1.0
0.5
0.0
**
*
AA - + + -
Rapamycin - - + +
C
Vehicle
LY294002
Rapamycin
Akt inhibitor I
Vehicle
AA

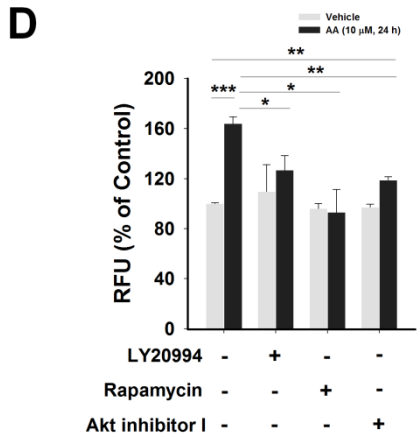

Figure 8. AA induces phosphorylation of Akt closely associated with mTORC2 signaling. **(A)** hUCB-MSCs were incubated with 10 μM of AA for various time periods (0 – 90 min). Total proteins were extracted and blotted with phosphor-Akt^{ser473}, phosphor-Akt^{thr308}, or Akt. **(B)** Cells were pre-treated with 10 nM of Rapamycin for 12 h prior to AA exposure for 60 min. Phosphor-Akt^{thr473} and Akt were detected by Western blotting. 10nM of Rapamycin (for 12 h), 10 μM of LY294002 (for 30 min), and 10 μM of Akt inhibitor I (for 30 min) were pre-treated to cells prior to 10 μM of AA incubation for 24 h. The inhibitory effect on the AA-enhanced hUCB-MSCs migration was examined in **(C)** wound healing assay and **(D)** Oris cell migration assay. (A-D) n = 3. Data represent means ± SE. *P< 0.05, **P< 0.01, ***P< 0.001. Scale bars = 100 μm

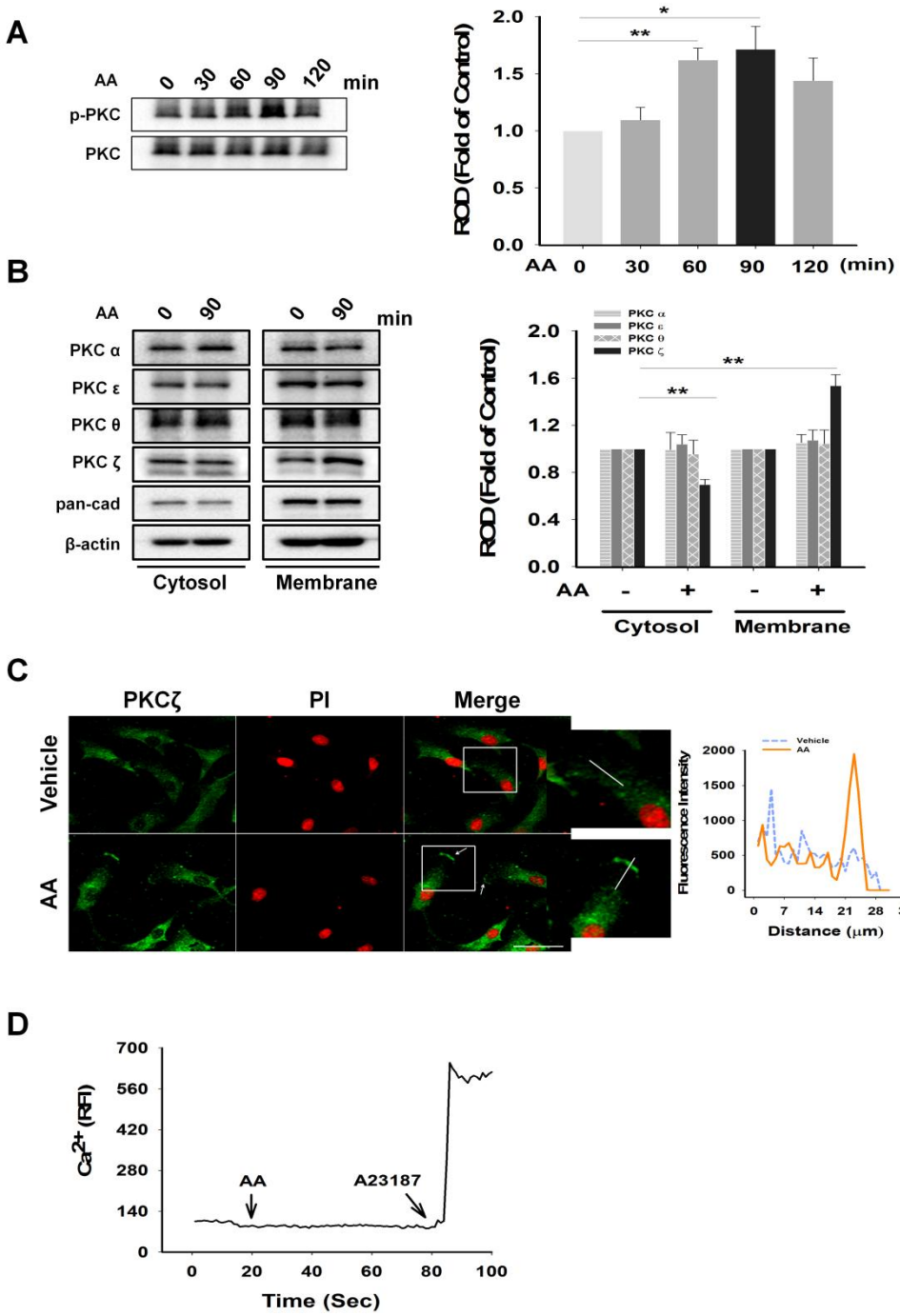
A
AA
0
30
60
90
120
min
p-PKC
PKC
ROD (Fold of Control)
2.0
1.5
1.0
0.5
0.0
*
**
AA 0 30 60 90 120 (min)
B
AA
0
90
0
90
min
PKC α
PKC ε
PKC θ
PKC ζ
pan-cad
β-actin
Cytosol
Membrane
PKC α
PKC ε
PKC θ
PKC ζ
ROD (Fold of Control)
2.0
1.6
1.2
0.8
0.4
0.0
**
**
AA - + - +
Cytosol
Membrane
C
PKCζ
PI
Merge
Vehicle
AA
Vehicle
AA
Fluorescence Intensity
2000
1500
1000
500
0
0 7 14 21 28 35
Distance (μm)
D
Ca2+ (RFI)
700
560
420
280
140
0
AA
A23187
0 20 40 60 80 100
Time (Sec)

Figure 9. AA stimulates atypical PKCζ translocation. (A) hUCB-MSCs were treated with 10 μM of AA for different time periods (0 – 120 min). Total cell lysates were analyzed by Western blotting using phospho-PKC and PKC antibodies. **(B)** Cells were stimulated with 10 μM of AA for 90 min and fractionated into cytosolic and membrane samples. Translocation of PKC isoforms were detected by Western blotting and pan-cadherin was used as a control for plasma membrane. **(C)** Cells incubated with 10 μM of AA for 90 min were immunostained with PKCζ antibody (green). PI was used for nuclear counterstaining (red). The arrows point to translocated PKCζ in plasma membrane by AA. And the right graph presents distribution of PKCζ on the yellow lines in the merged images, which were analyzed by FluoVeiwTM 300 software (Olympus, Tokyo, Japan). **(D)** Cells were loaded with 2 μM of Fluo-3/AM in serum free medium for 40 min and treated with 10 μM of AA. Ca^{2+} influx was investigated by confocal microscopy and data are expressed as relative fluorescence intensity (F/F0 %, arbitrary unit). A23187, a calcium ionophore, was used as a positive control. (A, B) n = 3. (C, D) n = 4. (A-D) Data represent means ± SE. $*P < 0.05$, $**P < 0.01$, $***P < 0.001$. Scale bars = 100 μm

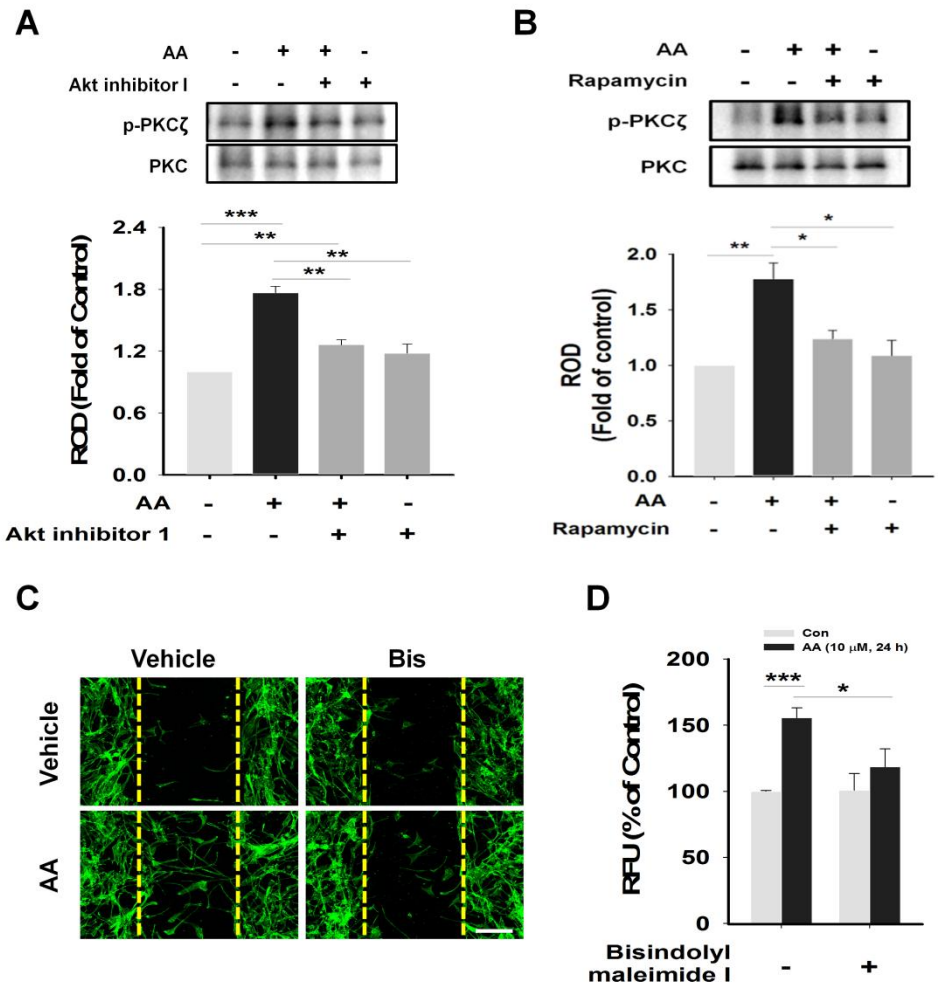

Figure 10. The activations of mTORC2 and Akt are responsible for phosphorylation of PKC in hUCB-MSCs treated with AA. (A, B) Cells pre-treated with 10 μM of Akt inhibitor I for 30 min or 10 nM of Rapamycin for 12 h were incubated with 10 μM of AA for 90 min. And phospho-PKCζ and PKC were detected by Western blotting. In **(C)** wound healing assay and **(D)** Oris cell migration assay, 5 μM of Bisindolylmaleimide I was pre-treated to cells for 30 min before treating AA (10 μM) for 24 h, and then their inhibitory effect on the AA-enhanced hUCB-MSCs migration was examined. (A- D) n = 3. Data represent means ± SE. *P< 0.05, **P< 0.01, ***P< 0.001. Scale bars = 100 μm

3. AA promotes MT3-MMP-mediated FN degradation through p38 MAPK/Sp1 cascade.

I analyzed the phosphorylation level of MAPKs, which are major PKC substrates.(Tang et al., 2012) AA uniquely induced phosphorylation of p38 MAPK from 60 to 120 min (Figure 11A), which was inhibited by pre-treatment with PKC inhibitor, Bisindolylmaleimide I (Figure 11B). But ERK and JNK were not stimulated by AA treatment. I then determined whether AA induces phosphorylation of Sp1, which is a ubiquitous transcription factor that controls gene expression involved in stem cell behavior.(Jeon et al., 2013) AA induced the phosphorylation of Sp1 from 6 to 12 h (Figure 12A) while no increase was observed before 6 h (data not shown). In addition, the nuclear translocation of Sp1 was observed at 6 h, and the translocation of Sp1 were blocked by pre-treatment with p38 MAPK inhibitor, SB203580 (Figure 12B). Furthermore, pre-treatment with SB203580, PI3K inhibitor (LY294002) and mTOR inhibitor (rapamycin) also blocked the phosphorylation of Sp1 induced by AA (Figure 13A-C). I also found that AA-induced cell motility was inhibited by SB203580 and Sp1 inhibitor,

Mithramycin A, in an *in vitro* wound-healing migration assay (Figure 14A) and in an Oris cell migration assay (Figure 14B).

As Sp1 is responsible for transcription of many MMP isotypes, which are crucial for cell migration,(Clark et al., 2008) mRNA levels of *MMP*s were analyzed with real-time PCR. Among *MMP* isotypes expressed in hUCB-MSCs,(Yun et al., 2014b) AA distinctively increased the mRNA levels of *MMP-12* and *MT3-MMP*, and decreased *MMP-11* and *MT1-MMP* (Figure 15A). AA also increased the protein expression of MT3-MMP, but did not alter the protein level of MMP-12 (Figure 15B). Additionally, I observed the increased protein level of MT3-MMP in the both cytosol and membrane with Western blotting and immunofluorescence staining (Figure 16A, B). Interestingly, I found that the gelatinolytic activity of MT3-MMP was enhanced by AA treatment (Figure 16C), suggesting that AA promotes the expression of MT3-MMP as well as its activity in hUCB-MSCs. The upregulation of MT3-MMP was abolished by Mithramycin A, Sp1 inhibitor (Figure 16D). To determine the effect of MT3-MMP on extracellular matrix (ECM) degradation, I analyzed protein levels of FN and COLs, which are major components of ECM. Under a state of uniform expression of those proteins in whole-cell lysates, AA uniquely induced FN

degradation from 12 to 24 h while there were no significant changes in COL−1, −3, and −5 in the medium (Figure 17A). By transfecting hUCB−MSCs with *MT3−MMP*siRNA, I observed the abolishment of AA−induced not just FN degradation, but also cell migration (Figure 17B−D).

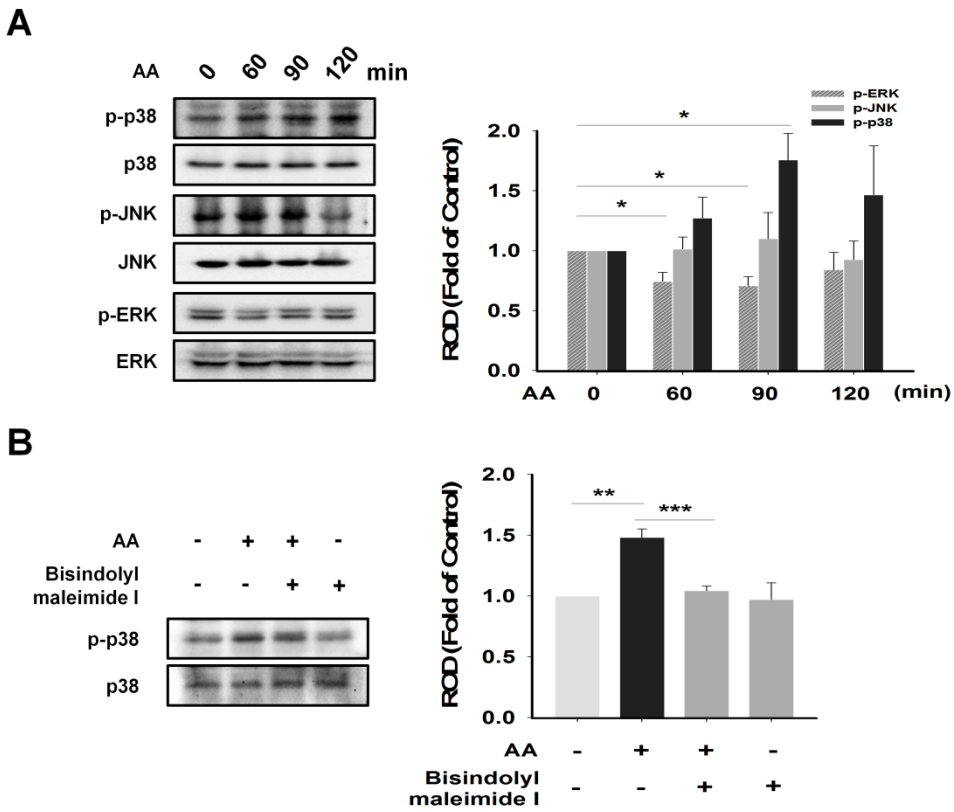

Figure 11. AA promotes phosphorylation of p38 MAPK. (A) hUCB-MSCs were treated with 10 μM of AA at various time points (0-120 min). Total cell lysates were blotted with phospho-ERK, -JNK, -p38 MAPK, and their total form. **(B)** Cells pre-treated with 5 μM of Bisindolylmaleimide I for 30 min were incubated with 10 μM of AA for 90 min. And phospho-p38 and p38 MAPK were detected by western blotting. (A, B) n=3. Data represent means±S.E. $*P<0.05$, $**P<0.01$, $***P<0.001$

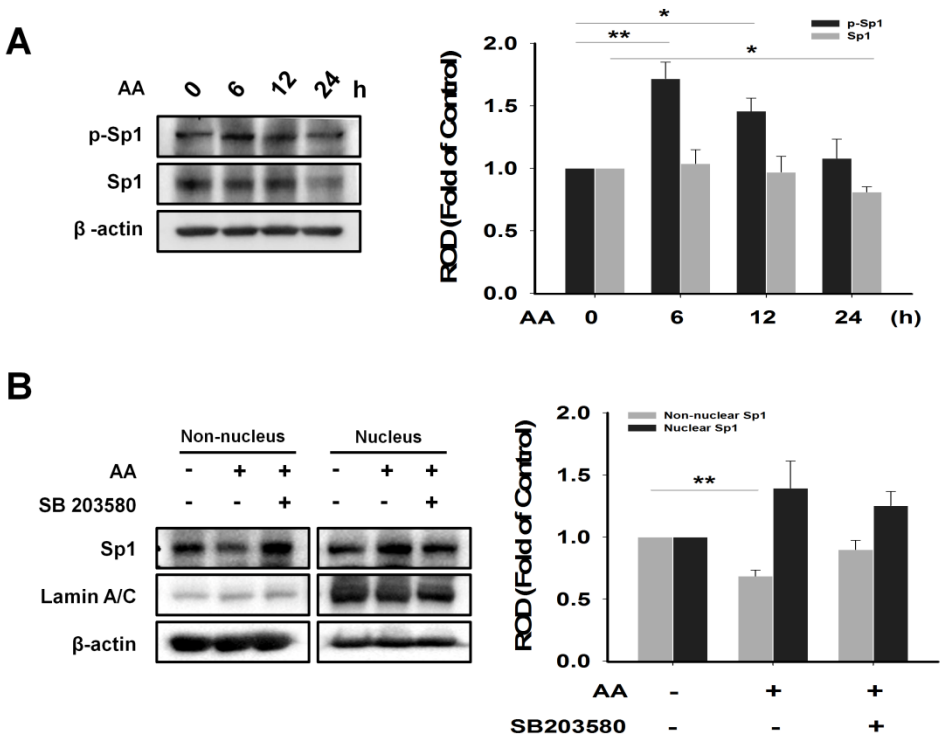

Figure 12. AA-induced phosphorylation of p38 MAPK is involved in Sp1 activation. (A) Cells were exposed to 10 μM of AA for different times (0-24 h), and then total proteins were extracted and examined with phospho-Sp1, Sp1, and β-actin antibodies by western blotting. (B) Cells were pre-treated with 1 μM of SB203580 for 30 min prior to 10 μM of AA incubation for 6 h and fractionated into non-nuclear and nuclear samples. Translocation of Sp1 was blotted, and the Lamin A/C was used as a control for nucleus. (A, B) n=3. Data represent means ± S.E. *P< 0.05, **P< 0.01, ***P< 0.001

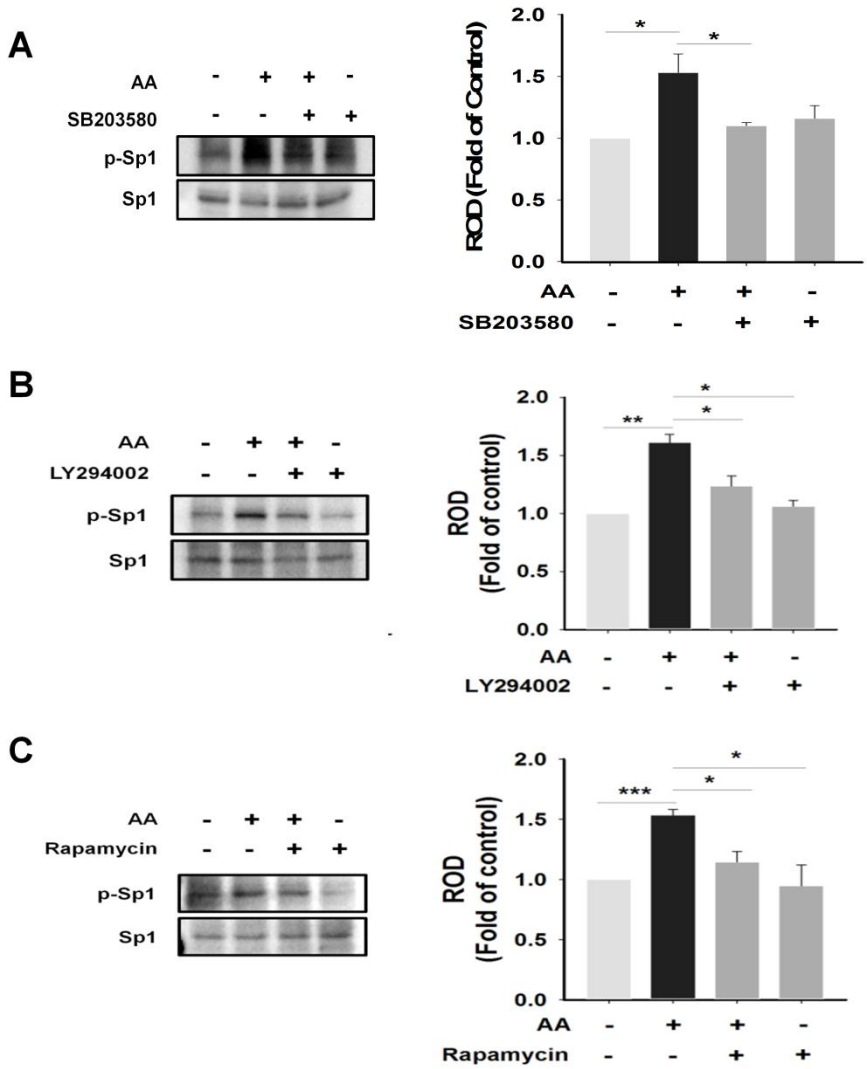

Figure 13. The activations of PIK3, mTORC2 and p38 MAPK are responsible for phosphorylation of Sp1 in hUCB-MSCs treated with AA. (A-C) The cells were pre-treated with 1 μM of SB203580 (for 30 min),10μM of LY294002 (for 30 min) or 10 nM of Rapamycin (for 12 h) prior to 10 μM of AA incubation. Phosphorylation of Sp1 was detected by Western blotting. n = 3. Data represent means ± SE. *P< 0.05, **P< 0.01, ***P< 0.001

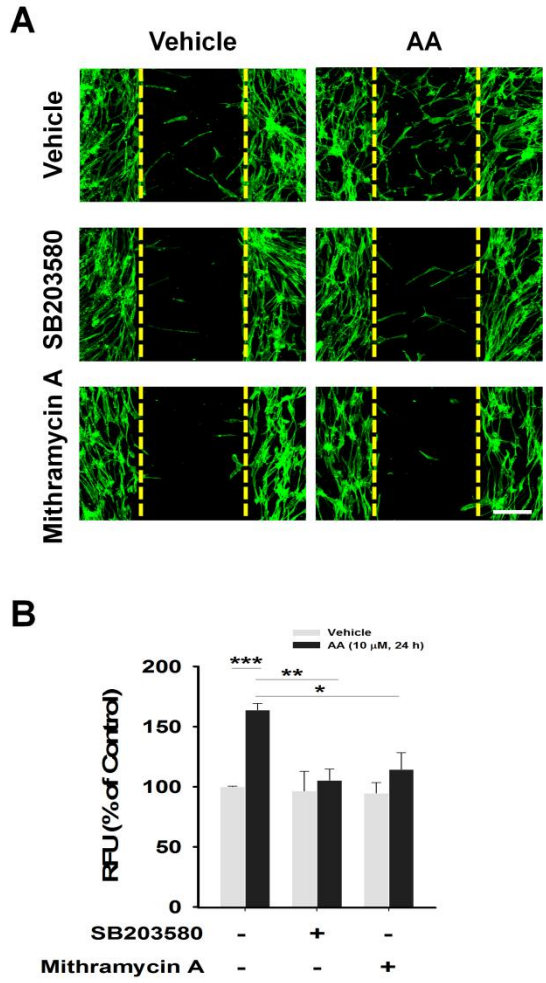

Figure 14. Involvements of p38 MAPK and Sp1 in AA-induced hUCB-MSC migration. In **(A)** wound healing assay and **(B)** Oris cell migration assay 1 μM of SB203580 and 5 μM of Mithramycin A were pre-treated to cells for 30 min before treating 10 μM of AA for 24 h, and then their inhibitory effect on the AA-enhanced hUCB-MSCs migration was examined. (A, B) n=3. Data represent means±S.E. *P< 0.05, **P< 0.01, ***P< 0.001. Scale bars = 100 μm

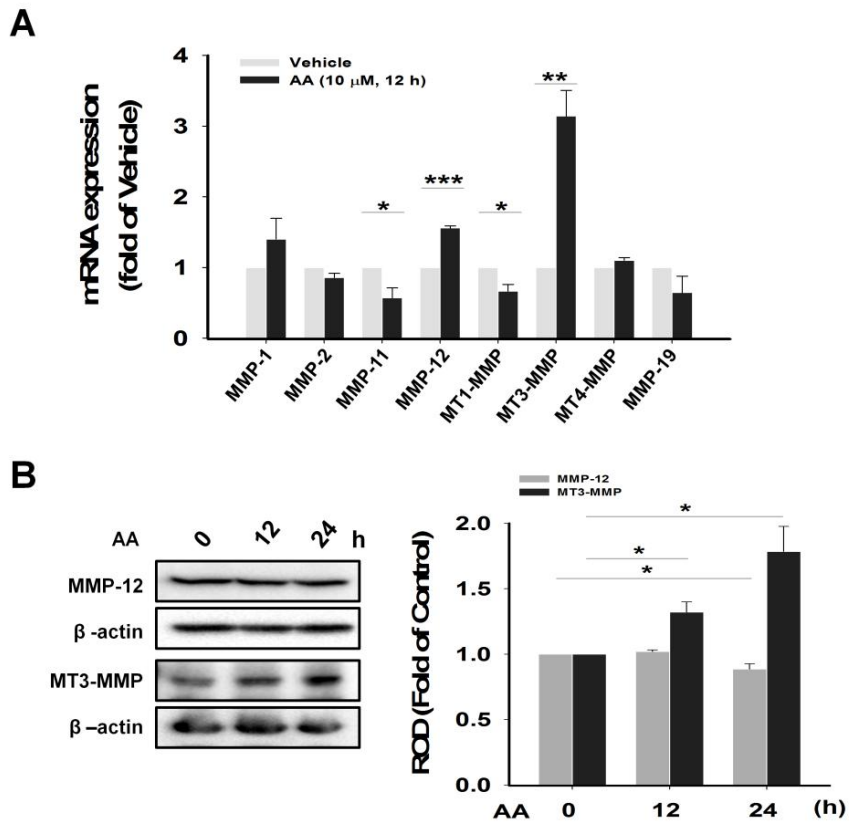

Figure 15. AA stimulates MT3-MMP expression. (A) With real-time PCR, the mRNA expression of *MMP* family was analyzed in hUCB-MSCs treated with10 μM of AA for 12 h. **(B)** Cells were exposed to 10 μM of AA for different time periods (0–24 h), and total cell lysates were subjected to SDS-PAGE for detecting MMP-12 and MT3-MMP. (A, B) n=3. Data represent means±S.E. *P< 0.05, **P< 0.01, ***P< 0.001

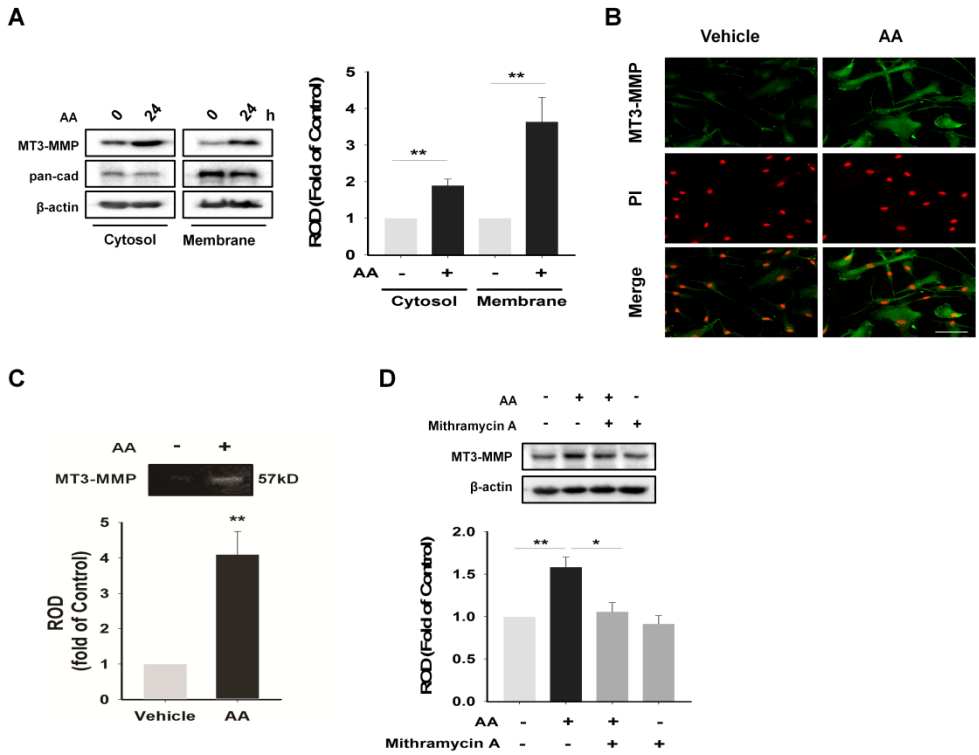

Figure 16. AA enhances translocation and enzymatic activity of MT3-MMP in hUCB-MSCs. (A) Cells were incubated with 10 μM of AA for 24 h and fractionated into cytosolic and membrane samples. Translocation of MT3-MMP was detected by western blotting, and pan-cadherin was used as a control for plasma membrane. (B) Cells treated with 10 μM of AA for 24 h were immunostained with MT3-MMP antibody (green). PI was used for nuclear counterstaining (red). (C) hUCB-MSCs were treated with 10 μM of AA for 24 h. Enzymatical activity of MT3-MMP was examined by using gelatin zymography. (D) Cells were pre-treated with 5 μM of Mithramycin for 30 min prior to 10 μM of AA exposure for 24 h. Then, total proteins were extracted and examined with MT3-MMP antibody by western blotting. (A, C, D) n=3. (B) n=5. Data represent means±S.E. *P< 0.05, **P< 0.01. Scale bars= 100 μm

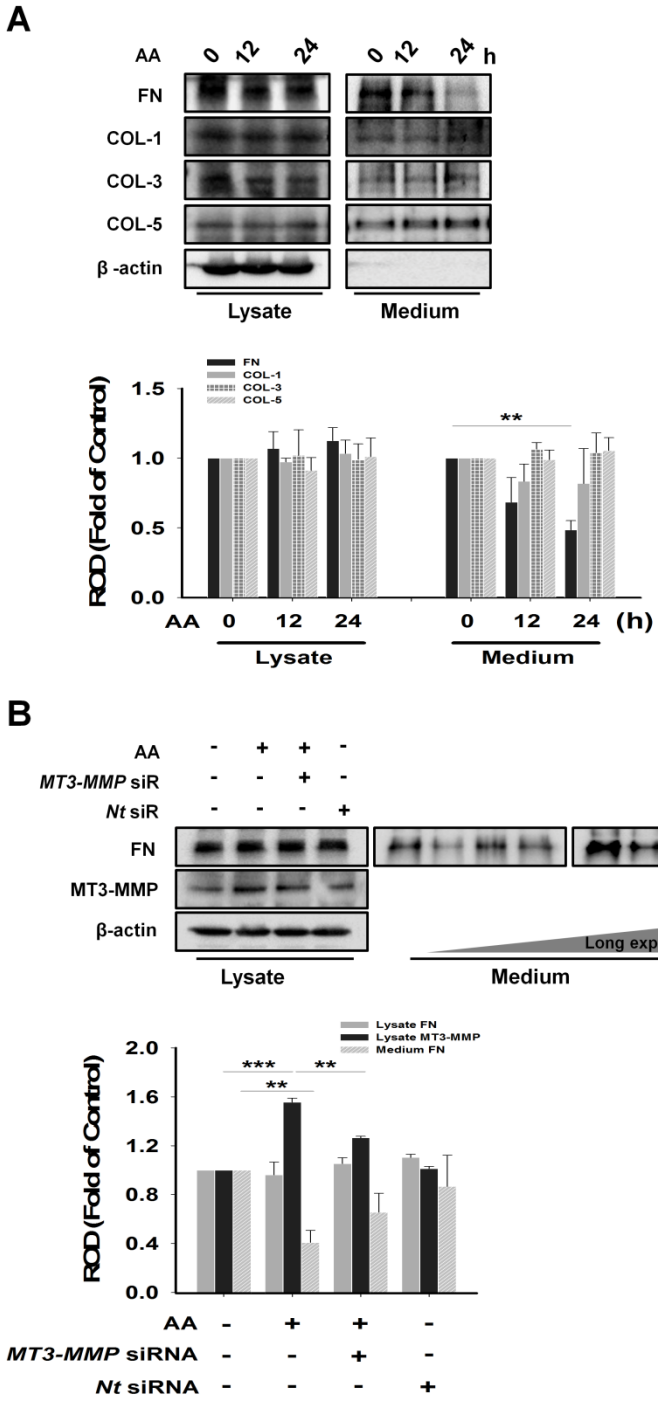
A
AA
0 12 24 0 12 24 h
FN
COL-1
COL-3
COL-5
β -actin
Lysate
Medium
FN
COL-1
COL-3
COL-5
ROD (Fold of Control)
1.5
1.0
0.5
0.0
**
AA 0 12 24 0 12 24 (h)
Lysate
Medium
B
AA - + + -
MT3-MMP siR - - + -
Nt siR - - - +
FN
MT3-MMP
β-actin
Long exposure
Lysate
Medium
Lysate FN
Lysate MT3-MMP
Medium FN
ROD (Fold of Control)
2.0
1.6
1.2
0.8
0.4
0.0
***
**
**
AA - + + -
MT3-MMP siRNA - - + -
Nt siRNA - - - +

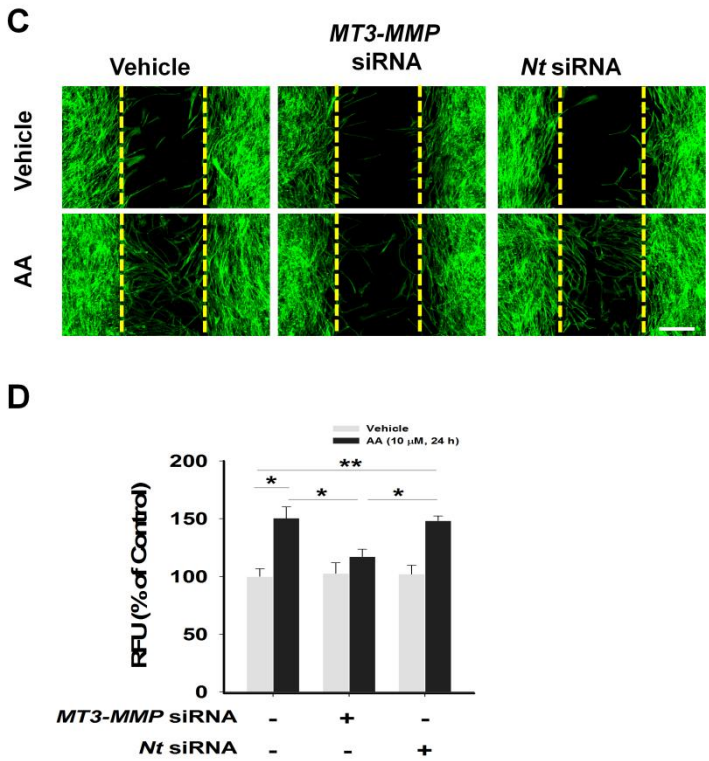

Figure 17. AA-upregulated MT3-MMP induces FN degradation and hUCB-MSCs migration. (A) Cells were treated with 10 μM of AA for 24 h. Western blot assay of FN, COL-1, COL-3, and COL-5 on both cell lysates and proteins precipitated from medium by 30% trichloroethanoic acid was carried out. **(B)** Cells were transfected with *MT3-MMP*siRNA (25 nM) for 24 h prior to 10 μM of AA incubation for 24 h. And protein levels of FN both in cell lysates and in medium were analyzed with western blotting. In **(C)** wound healing assay and **(D)** Oris cell migration assay, *MT3-MMP* specific siRNA (25 nM) were transfected to cells for 24 h prior to 10 μM of AA treatment for 24 h. And then, we examined the inhibitory effect of knockdown of MT3-MMP on the cell migration. (A, B) n=3. (C, D) n=4. Data represent means±S.E. *P< 0.05, **P< 0.01, ***P< 0.001. Scale bars=100 μm

4. AA-upregulated MT3-MMP stimulates the skin wound healing effect of hUCB-MSCs.

In experiments to determine whether AA-upregulated MT3-MMP contributes to the skin wound healing effect of hUCB-MSCs, the hUCB-MSCs/*non-targetring (Nt)* siRNA induced a better wound-healing effect than that of hUCB-MSCs/*MT3-MMP*siRNA in the mouse model with gross evaluation at day 5 (Figure 18A). In addition, hUCB-MSCs/*Nt*siRNA pre-treated with AA had a better effect than with vehicle up to 20% at day 9 (Figure 18A). Furthermore, I found that hUCB-MSCs/*Nt*siRNA pre-treated with AA induced more vessels around the wound, and the knockdown of MT3-MMP resulted in an inhibitory effect on angiogenesis in gross examination of neovasculature (Figure 18B). Histological evaluation of H&E stained skin wounds showed that all groups (except for the hUCB-MSCs/*Nt*siRNA pre-treated with AA) had imperfect wound closure or granulation which did not make intimate contact with the surrounding tissue and had less hair follicle density in recovered wound area (Figure 18C). To evaluate how many transplanted cells migrated to the wound site for restoration, I counted BrdU-stained

hUCB-MSCs at the site and found that the number of the hUCB-MSCs/*Nt*siRNA pre-treated with AA was more than that of the other groups by 70% (Figure 19A). In addition, I confirmed the majority of BrdU-labeled cells in wound tissues were not co-localized with endothelial cells marker, CD34, indicating that exogenous hUCB-MSCs did not seem to be differentiated into endothelial cells (Figure 19B).

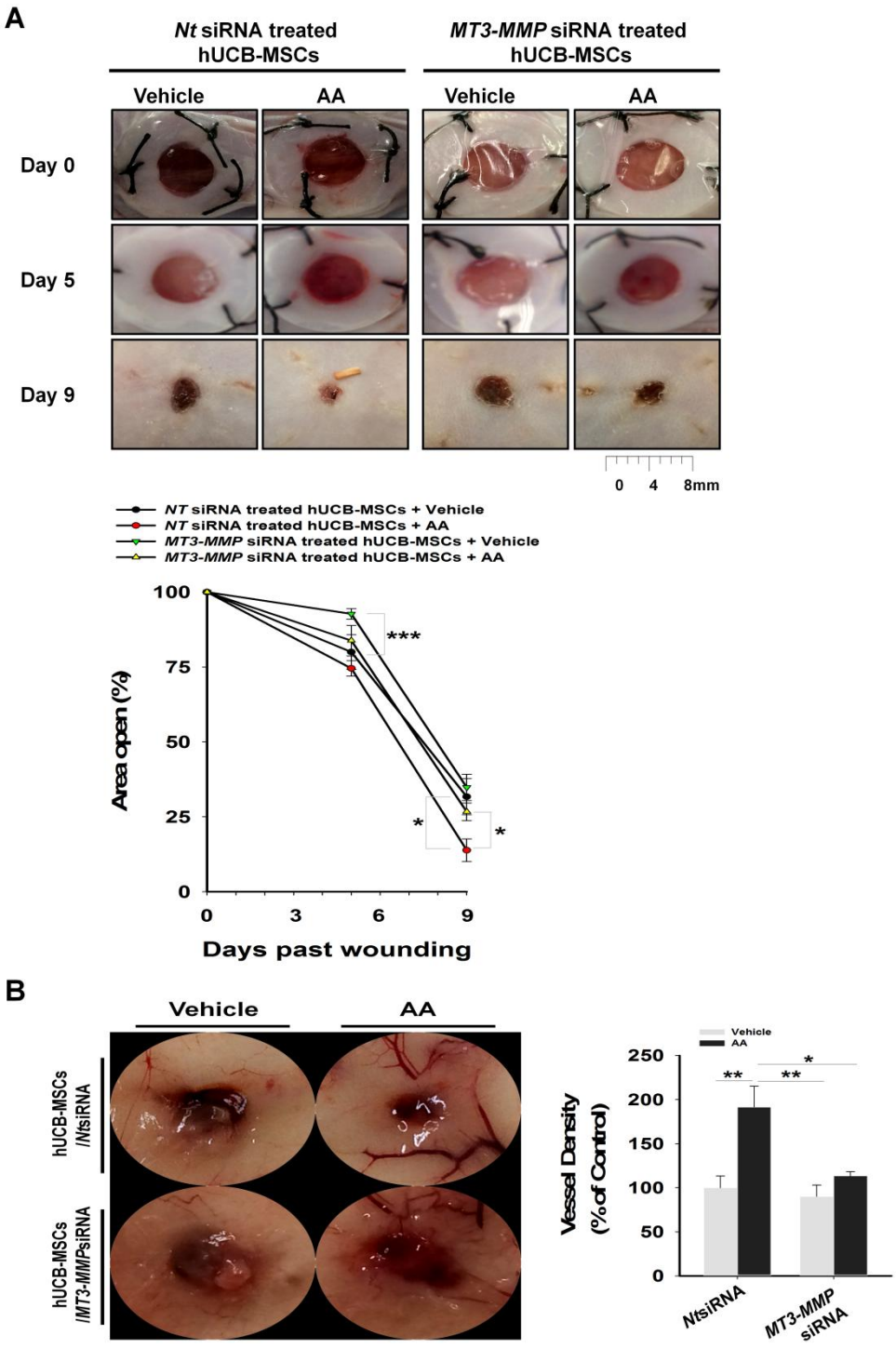
A
Nt siRNA treated hUCB-MSCs
MT3-MMP siRNA treated hUCB-MSCs
Vehicle
AA
Vehicle
AA
Day 0
Day 5
Day 9
0 4 8mm
NT siRNA treated hUCB-MSCs + Vehicle
NT siRNA treated hUCB-MSCs + AA
MT3-MMP siRNA treated hUCB-MSCs + Vehicle
MT3-MMP siRNA treated hUCB-MSCs + AA
Area open (%)
100
75
50
25
0
0
3
6
9
Days past wounding
***
*
*
B
Vehicle
AA
hUCB-MSCs /NtsiRNA
hUCB-MSCs /MT3-MMPsiRNA
Vessel Density (%of Control)
Vehicle
AA
250
200
150
100
50
0
**
**
*
NtsiRNA
MT3-MMP siRNA

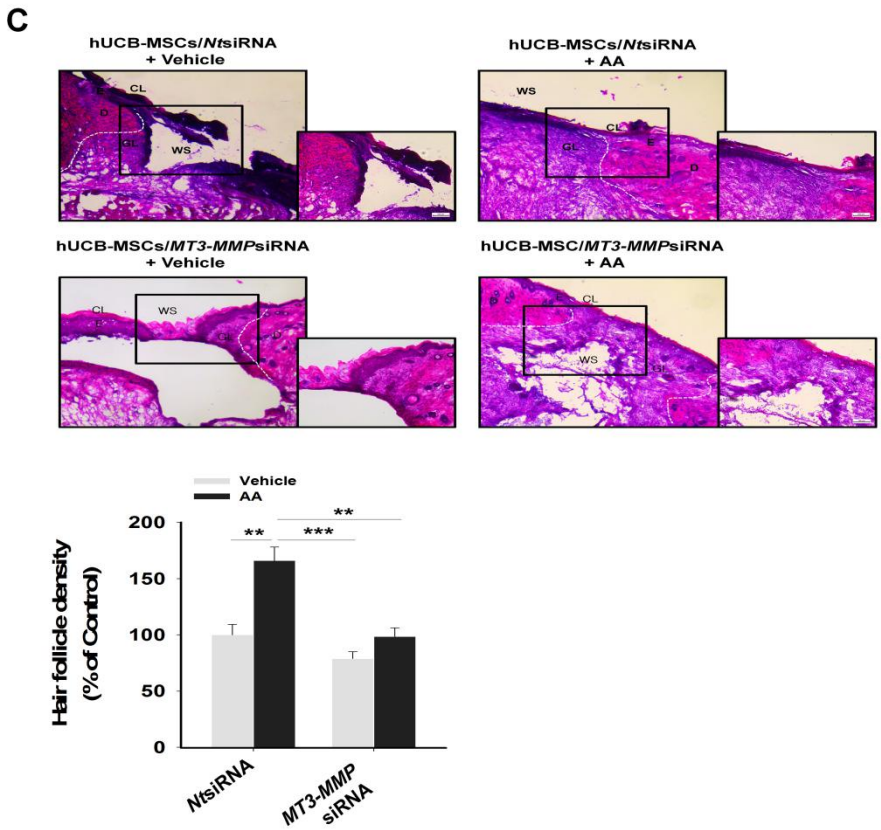

Figure 18. AA-upregulated MT3-MMP affects skin wound healing. Wounds were made with the same way used in Figure 1 and transplanted with hUCB-MSCs/*MT3-MMP*siRNA (25 nM) or hUCB-MSCs/*Nt*siRNA (25 nM), which were divided into groups pre-treated with AA (10 μM) or vehicle respectively. **(A)** Representative images of mouse cutaneous wounds on postoperative days are shown. Open wound areas relative to the original wound size were quantified with Image J program. **(B)** Representative images of neovasculature in wounds at day 9. Vessel densities relative to the group treated with Vehicle alone were quantified with Image J program. **(C)** Representative H&E sections of wound tissues at day 9 are shown. Hair follicle densities relative to the group treated with Vehicle were quantified. (A-C) n = 5. Scale bars = 100 μm. Data represent means ± SE. $*P<0.05$, $**P<0.01$, $***P<0.001$

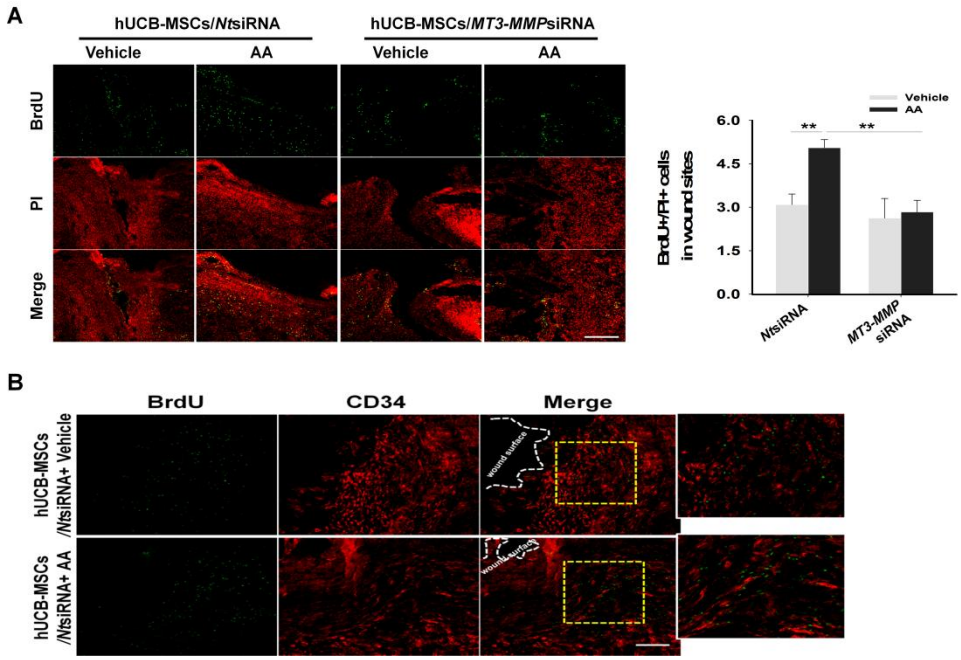

Figure 19. AA promotes hUCB-MSCs to migrate into the wound sites without differentiation. BrdU-labeled hUCB-MSCs were topically implanted onto the wound bed and injected into the dermis of the surrounding skin. In wound site at day 9, the labeled hUCB-MSCs were determined with confocal microscopy. BrdU was stained with immunofluorescence antibody (green). **(A)** PI was used for nuclear counterstaining (red). **(B)** CD34 was used for the endothelial cell marker (red). (A) n=4. Scale bars = 200 μm. (B) n=5. Scale bars = 100 μm. Data represent means ± SE. $^{**}P < 0.01$

DISCUSSION

In the present study, I demonstrated that AA enhances skin wound healing through the induction of hUCB-MSCs migration in which AA stimulates GPR40 coupling with mTORC2 signaling to regulate MT3-MMP-mediated FN degradation (Figure 20A). I first found that AA by itself has the ability to aid cutaneous wound repair, suggesting that application of AA might amplify the bioactivity of various migrating cells. In recent studies, some eicosanoids generated from AA in the wound area have been shown to induce proliferation and migration of various cells including keratinocytes and recruited stem cells for wound healing. (Berry et al., 2017; Sivamani. 2014) Consistently, the transplantation of hUCB-MSCs, pre-treated with AA, was shown to accelerate skin regeneration through tissue re-formation and blood vessel supply. The majority of mesenchymal stem cells has been shown to enhance the angiogenesis via the paracrine mechanism rather than the multilineage differentiation.(Kwon et al., 2013) Thus, it is possible

that AA induces motility of hUCB-MSCs to enhance the mobilization and recruitment of stem cells into wound site, where hUCB-MSCs activate paracrine mechanisms to promote vascular growth and angiogenesis.(Hocking & Gibran. 2010; Liu et al., 2014) Therefore, my results suggest that the pre-activation of the hUCB-MSCs with AA could potentiate cell transplantation therapy not only with timely efficacy, but also with reduction of the side effects of overdose of AA. In addition, the pre-activation of hUCB-MSCs with AA may offer a means of improving the potency of these cells without the need for additional cell numbers. It should be noted that the proper concentration of AA is critical to improve the outcome of stem cell treatment. In this study, I found that $\leq$ 10 μM of AA stimulates hUCB-MSCs migration in a dose- and time-dependent manner, but $\geq$ 15 μM of AA gradually decreases the migration. A similar result was also reported in which self-renewal of neural stem/progenitor cells diminished over a specific concentration of AA (10 μM).(Sakayori et al., 2011) These results show that the proper concentration of AA is crucial in stem cell-based therapy and that relatively large amounts of AA are a burden on adult stem/progenitor cells, which is closely associated with oxidative stress from lipid peroxidation.(Pompeia et al., 2002) In

this respect, AA levels are not just permissive for stem cell functions but also determinative for at least certain aspects of the functions.

Although the roles of $\omega-6$ PUFAs in proliferation and angiogenic effect of stem cells have been well studied,(Kim et al., 2009; Smith et al., 2012) the functional role of AA by itself in stem cell migration has not been elucidated. GPR40, a membrane receptor for $\omega-6$ PUFAs, is known to govern neurogenesis, nutrient sensing in the pancreas, inflammatory condition of the skin, and even proliferation of embryonic stem cells.(Boneva et al., 2011; Fujita et al., 2011; Kim et al., 2009; Tomita et al., 2014) In contrast to a previous report showing that some $\omega-6$ PUFAs could regulate cellular events by interacting with cytosolic effectors via diffusion, receptor, or transporters.(Brash. 2001; Fei et al., 2011) I found that AA directly promotes stem cell migration via GPR40, suggesting that the GPR40 activation is the critical requirement in improving the bioactivity of hUCB-MSCs for skin wound healing. mTOR, a pivotal regulator of cell metabolism and behaviors, integrates both extracellular and intracellular signals,(Gibbons et al., 2009) but the relationship between GPR40 and mTOR has not been investigated. In fact, my data revealed that GPR40-dependent

activation of the PI3K/mTORC2/Akt^{ser473} pathway has a key role in AA-induced hUCB-MSCs migration. However, the Akt^{thr308}/mTORC1 pathway was not involved in this process. These results are consistent with previous reports showing the distinctive role of mTORC1 and mTORC2.(Apte et al., 2013; Kim et al., 2011; Tang et al., 2014a) In those reports, the Akt^{thr308}/mTORC1 cascade mainly controlled cell growth, whereas cytoskeletal re-organization related to cell motility was critically regulated by the mTORC2/Akt^{ser473} cascade. Moreover, I showed that mTORC2 has the capacity to stimulate mTORC1 through Akt^{ser473} activation. Thus, my results suggest that mTORC2 is not only a major signaling hub in controlling AA-mediated hUCB-MSCs migration, but also a unique AA sensor that receives signals transduced from GPR40. This is further supported by a previous report describing that nutrient/redox/mitogenic input modulates the involvement mTORC2 signaling in cell movement.(Tang et al., 2014b) To the best of my knowledge, this is the first study to show the relationship between GPR40 and mTOR. These findings suggest that the physiological activation of mTORC2 may be required for proper skin wound healing and that further activation of other members of the mTORC2 signaling pathway may also be a viable strategy to influence skin

recovery.

It was previously documented that lysophosphatidic acid or amino acids induce mTORC2-mediated phosphorylation of Akt^{ser473}, PKC α, or PKC δ for cell migration.(Gan et al., 2012; Treins et al., 2010) In contrast, I revealed that AA stimulates atypical (a) PKC ζ through mTORC2/Akt^{ser473} activation in enhancing hUCB-MSCs motility. This discrepancy could be explained by that ω-6 PUFAs are potent aPKC ζ stimulators.(Nakanishi et al., 1992) Indeed, ω-6 PUFAs were reported to promote oligonucleotide internalization through aPKC ζ activation.(Khaled et al., 1999) Thus, my data show that mTORC2 could transduce AA-induced signals to aPKC ζ via Akt^{ser473}. Having shown the functional role of aPKC ζ in hUCB-MSCs migration induced by AA, I further studied the mechanism on how aPKC ζ links to other key molecules in stem cell migration. Interestingly, AA through aPKC ζ selectively induced p38 MAPK-dependent activation of Sp1, which has the potential ability to modulate cell migration in response to some PUFAs.(Li et al., 2013; Park et al., 2009; Peng et al., 2013) However, both ERK and JNK were not stimulated by AA, suggesting a cell-specific role of AA in determining downstream targets. My results are further supported by a previous report showing that AA regulates both p38 MAPK and

ERK for transcriptional activation of the cAMP response element-binding protein (CREB) in driving vascular smooth muscle cell movement.(Chava et al., 2009) Although MAPKs have been documented to be capable of controlling the transcriptional activity of Sp1,(Curry et al., 2008; Ohoka et al., 2014) the activation of Sp1 occurred long after that of p38 MAPK. This result is probably due to O-glycosylation of Sp1 by p38 MAPK, which contributes to nuclear translocation in which the Sp1 is phosphorylated.(Cheung et al., 2008; Jeon et al., 2013) Thus, my results indicate that Sp1 has an important role in hUCB-MSC migration by receiving the unique AA signaling pathway. Here, I show for the first time that the addition of AA had beneficial effects, improving the quality of hMSCs generated from cord blood through AA-induced bioactive signaling molecules.

During wound regeneration, MMPs remodel the ECM, allowing the penetration of stem cells and blood vessels into the wound site for tissue repair.(Bellayr et al., 2013; Ghajar et al., 2008) Although MT-MMPs have been reported to dissolve the basement membrane directly and promote adult stem/progenitor cell motility,(Liu et al., 2012; Noel et al., 2008; Strong et al., 2012; Sun et al., 2013) their functional role in stem cell migration and their effects on skin

wound healing have not been characterized. In the present study, I found that AA uniquely increases the level of MT3-MMP among all the isoforms of MMP to regulate ECM degradation. In contrast to previous reports showing that secretory MMP-12 participates in the mobilization of hUCB-MSCs in response to some microenvironmental factors,(Lee et al., 2014a; Yun et al., 2014b) I identified that AA exclusively upregulates MT3-MMP through Sp1 in promoting the motility of hUCB-MSCs. This implies that the activation of MMPs is distinctively regulated by microenvironmental factors that affect the transcription of many MMP isotypes. Despite the fact that MT3-MMP could degrade FN and COL-3 among the ECM proteins,(Matsumoto et al., 1997) I found that AA-upregulated MT3-MMP uniquely degraded FN which is abundant during the stage of granulation and angiogenesis during wound repair.(Repesh et al., 1982) This FN targeting proteolysis is considered due to cell surface ECM adhesion proteins such as integrin, however, further study is needed to clarify. It has been documented that MT3-MMP modifies the pericellular ECM, allowing the cells to have more functional podia highly specialized for migration.(Moss et al., 2009) The results highlight that MT3-MMP specifically mediates the motility of hUCB-MSCs induced by

AA.

Consistently, I found that the silencing of the MT3-MMP in hUCB-MSCs pre-activated with AA failed to regulate stem cell motility, resulting in a significant delay in *in vivo* angiogenesis and wound healing despite the AA pre-treatment. This means that the phenotypic outcome of hUCB-MSCs induced by AA *in vitro* is well maintained during skin wound healing in mouse. As MT3-MMP is a membrane-bound metalloproteinase and not a secreted one, I thought that MT3-MMP itself does not directly regulate angiogenesis *in vivo*. Instead, MT3-MMP plays a critical role in promoting the motility of hUCB-MSCs. Thus, it is possible that MT3-MMP cleaves pericellular substrate including FN and could therefore allow cells to migrate into wound sites. These mean that AA controls surface restriction of MT3-MMP to specifically degrade FN in promoting the migration of stem cells into wound site where the hUCB-MSCs induce the angiogenesis via paracrine mechanism or enhance the skin wound healing with specific modes of action.

Taken together, my findings suggest that pre-activation of hUCB-MSCs would provide new methods for stem cell therapy in wound healing and contribute to rationally develop culture conditions with

optimal AA concentration or AA-based intervention protocols that could lead to long-term cost-effective outcomes in hUCB-MSC-based skin wound therapy. In conclusion, AA promotes skin wound healing through induction of hUCB-MSC motility for which AA binding to GPR40 stimulates the PI3K/mTORC2/Akt^{ser473}/PKC ζ/p38 MAPK/Sp1 cascade leading to MT3-MMP-dependent FN degradation.

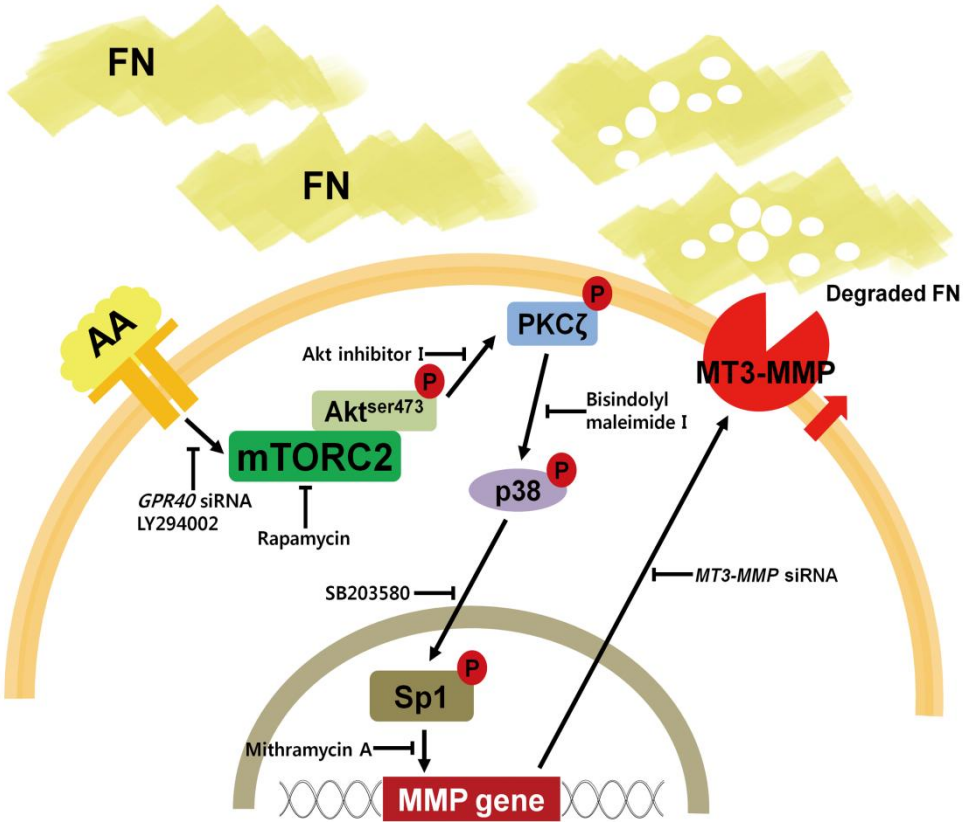

Figure 20. A hypothetical model for AA-induced signaling pathway in promoting hUCB-MSCs migration.

REFERENCES

Apte SA., Cavazos DA., Whelan KA., and Degraffenried LA. (2013). A low dietary ratio of ω-6 to ω-3 fatty acids may delay progression of prostate cancer. Nutr Cancer. 65, 556-562.

Bellayr I., Holden K., Mu X., Pan H., and Li Y. (2013). Matrix metalloproteinase inhibition negatively affects muscle stem cell behavior. Int J Clin Exp Pathol. 6, 124-141.

Berry E., Liu Y., Chen L., Guo AM. (2017). Eicosanoids: Emerging contributors in stem cell-mediated wound healing. Prostag Oth Lipid M. 132, 17-24.

Black AK., Fincham N., Greaves MW., and Hensby CN. (1981). Time course changes in levels of arachidonic-acid and prostaglandins D2, E2, F2-α in human skin following ultraviolet B irradiation. Br J Clin Pharmacol. 10, 453-457.

Boneva NB., Kikuchi M., Minabe Y., and Yamashima T. (2011). Neuroprotective and ameliorative actions of polyunsaturated fatty acids against neuronal diseases: implication of fatty acid-binding proteins (FABP) and G protein-coupled receptor 40 (GPR40) in adult neurogenesis. J Pharmacol Sci. 116, 163-172.

Bradford MM. (1976). A rapid and sensitive method for the

quantitation of microgram quantities of protein utilizing the principle of protein-dye binding. Anal Biochem. 72, 248-254.

Brash AR. (2001). Arachidonic acid as a bioactive molecule. J Clin Invest. 107, 1339-1345.

Castilho RM., Squarize CH., and Gutkind JS. (2013). Exploiting PI3K/mTOR signaling to accelerate epithelial wound healing. Oral Dis. 19, 551-558.

Castilho RM., Squarize CH., Leelahavanichkul K., Zheng Y., Bugge T., and Gutkind JS. (2010). Rac1 is required for epithelial stem cell function during dermal and oral mucosal wound healing but not for tissue homeostasis in mice. PLoS One.5, e10503.

Chava KR., Karpurapu M., Wang D., Bhanoori M., Kundumani-Sridharan V., Zhang Q., Ichiki T., Glasgow WC., and Rao GN. (2009). CREB-mediated IL-6 expression is required for 15(S)-hydroxyeicosatetraenoic acid-induced vascular smooth muscle cell migration. Arterioscl Throm Vas. 29, 809-815.

Cheung WD., and Hart GW. (2008). AMP-activated protein kinase and p38 MAPK activate O-GlcNAcylation of neuronal proteins during glucose deprivation. J Biol Chem. 283, 13009-13020.

Clark IM., Swingler TE., Sampieri CL., and Edwards DR. (2008). The regulation of matrix metalloproteinases and their inhibitors. Int J Biochem Cell Biol. 40, 1362-1378.

Curry JM., Eubank TD., Roberts RD., Wang YJ., Pore N., Maity A., and Marsh CB. (2008). M-CSF signals through the MAPK/ERK pathway via Sp1 to induce VEGF production and induces

angiogenesis *in vivo*. Plos One. 3,

Ennis WJ., Sui A., and Bartholomew A. (2013). Stem cells and healing: impact on inflammation. Adv Wound Care (New Rochelle). 2, 369-378.

Fei J., Cook C., Gillespie M., Yu B., Fullen K., and Santanam N. (2011). Atherogenic ω-6 lipids modulate PPAR-EGR-1 crosstalk in vascular cells. PPAR Res. 2011, 753917.

Fujita T., Matsuoka T., Honda T., Kabashima K., Hirata T., and Narumiya S. (2011). A GPR40 agonist GW9508 suppresses CCL5, CCL17, and CXCL10 induction in keratinocytes and attenuates cutaneous immune inflammation. J Invest Dermatol. 131, 1660-1667.

Gan X., Wang J., Wang C., Sommer E., Kozasa T., Srinivasula S., Alessi D., Offermanns S., Simon MI., and Wu D. (2012). PRR5L degradation promotes mTORC2-mediated PKC-σ phosphorylation and cell migration downstream of $G\alpha_{12}$. Nat Cell Biol. 14, 686-696.

Gartner A., Pereira T., Armada-da-Silva P., Amado S., Veloso A., Amorim I., Ribeiro J., Santos J., Barcia R., Cruz P., Cruz H., Luis A., Santos J., Geuna S., and Mauricio A. (2014). Effects of umbilical cord tissue mesenchymal stem cells (UCX®) on rat sciatic nerve regeneration after neurotmesis injuries. J Stem Cells Regen Med. 10, 14-26.

GhajarCM., George SC., and Putnam AJ. (2008). Matrix metalloproteinase control of capillary morphogenesis. Crit Rev Eukar Gene. 18, 251-278.

Gibbons JJ., Abraham RT., and Yu K. (2009). Mammalian target of rapamycin: discovery of rapamycin reveals a signaling pathway important for normal and cancer cell growth. Semin Oncol. 36 Suppl 3, S3-S17.

Hocking AM., and Gibran NS. (2010). Mesenchymal stem cells: paracrine signaling and differentiation during cutaneous wound repair. Exp Cell Res. 316, 2213-2219.

Jacobi SK., MoeserAJ., Corl BA., Harrell RJ., Blikslager AT., and Odle J. (2012). Dietary long-chain PUFA enhance acute repair of ischemia-injured intestine of suckling pigs. J Nutr. 142, 1266-1271.

Jeon JH., Suh HN., Kim MO., and Han HJ. (2013). Glucosamine-induced reduction of integrin $\beta 4$ and plectin complex stimulates migration and proliferation in mouse embryonic stem cells. Stem Cells Dev. 22, 2975-2989.

Kang JX., and Liu A. (2013). The role of the tissue ω-6/ω-3 fatty acid ratio in regulating tumor angiogenesis. Cancer Metast Rev. 32, 201-210.

Khaled Z., Ho YY., Benimetskaya L., DeckelbaumRJ., and Stein CA. (1999). ω-6 polyunsaturated fatty acid-stimulated cellular internalization of phosphorothioate oligodeoxynucleotides: evidence for protein kinase C-ζ dependency. Biochem Pharmacol. 58, 411-423.

Kim EK., Yun SJ., Ha JM., Kim YW., Jin IH., Yun J., Shin HK., Song SH., Kim JH., Lee JS., Kim CD., and Bae SS. (2011). Selective activation of Akt1 by mammalian target of rapamycin complex 2

regulates cancer cell migration, invasion, and metastasis. Oncogene. 30, 2954-2963.

Kim HS., Shin TH., Lee BC., Yu KR., Seo Y., Lee S., Seo MS., Hong IS., Choi SW., Seo KW., Nunez G., Park JH., and Kang KS. (2013). Human umbilical cord blood mesenchymal stem cells reduce colitis in mice by activating NOD2 signaling to COX2. Gastroenterology. 145, 1392-1403.

Kim MH., Kim MO., Kim YH., Kim JS., and Han HJ. (2009). Linoleic acid induces mouse embryonic stem cell proliferation via Ca^{2+}/PKC, PI3K/Akt, and MAPKs. Cell Physiol Biochem. 23, 53-64.

Kwon YW., Heo SC., Jeong GO., Yoon JW., Mo WM., Lee MJ., Jang IH., Kwon SM., Lee JS., and Kim JH. (2013). Tumor necrosis factor-α-activated mesenchymal stem cells promote endothelial progenitor cell homing and angiogenesis. Biochim Biophys Acta. 1832, 2136-2144.

Lee SJ., Jung YH., Oh SY., Yong MS., Ryu JM., and Han HJ. (2014a). Netrin-1 induces MMP-12-dependent E-Cadherin degradation via the distinct activation of PKCα and FAK/Fyn in promoting mesenchymal stem cell motility. Stem Cells Dev. 23, 1870-1882.

Lee SJ., Jung YH., Oh SY., Yun SP., and Han HJ. (2014b). Melatonin enhances the human mesenchymal stem cells motility via melatonin receptor 2 coupling with Gαq in skin wound healing. J Pineal Res. 57, 393-407.

Li X., and Tai HH. (2013). Activation of thromboxane A2 receptor (TP) increases the expression of monocyte chemoattractant protein -1 (MCP-1)/chemokine (C-C motif) ligand 2 (CCL2) and recruits

macrophages to promote invasion of lung cancer cells. PLoS One.8, e54073.

Limova M. (2010). Active wound coverings: bioengineered skin and dermal substitutes. Surg Clin North Am. 90, 1237-1255.

Liu J., van Mil A., Aguor ENE., Siddiqi S., Vrijsen K., Jaksani S., Metz C., Zhao JJ., Strijkers GJ., Doevendans PA., and Sluijter JPG. (2012). MiR-155 inhibits cell migration of human cardiomyocyte progenitor cells (hCMPCs) via targeting of MMP-16. J Cell Mol Med. 16, 2379-2386.

Liu L., Yu Y., Hou Y., Chai J., Duan H., Chu W., Zhang H., Hu Q., and Du J. (2014). Human umbilical cord mesenchymal stem cells transplantation promotes cutaneous wound healing of severe burned rats. PLoS One.9, e88348.

Martinez-Orozco R., Navarro-Tito N., Soto-Guzman A., Castro-Sanchez L., and Perez Salazar E. (2010). Arachidonic acid promotes epithelial-to-mesenchymal-like transition in mammary epithelial cells MCF10A. Eur J Cell Biol. 89, 476-488.

Matsumoto SI., Katoh M., Saito S., Watanabe T., and Masuho Y. (1997). Identification of soluble type of membrane-type matrix metalloproteinase-3 formed by alternatively spliced mRNA. Biochim Biophys Acta. 1354, 159-170.

Moss NM., Wu YI., Liu YY., Munshi HG., and Stack MS. (2009). Modulation of the membrane type 1 matrix metalloproteinase cytoplasmic tail enhances tumor cell invasion and proliferation in three-dimensional collagen matrices. J Biol Chem. 284, 19791-19799.

Nakanishi H., and Exton JH. (1992). Purification and characterization of the ζ isoform of protein kinase C from bovine kidney. J Biol Chem. 267, 16347-16354.

Noel A., Jost M., and Maquoi E. (2008). Matrix metalloproteinases at cancer tumor-host interface. Semin Cell Dev Biol. 19, 52-60.

Ohoka Y., Yokota-Nakatsuma A., Maeda N., Takeuchi H., and Iwata M. (2014). Retinoic acid and GM-CSF coordinately induce retinal dehydrogenase 2 (RALDH2) expression through cooperation between the RAR/RXR complex and Sp1 in dendritic cells. PLoS One.9, e96512.

Park MH., Ahn BH., Hong YK., and Min do S. (2009). Overexpression of phospholipase D enhances matrix metalloproteinase-2 expression and glioma cell invasion via protein kinase C and protein kinase A/NF-κB/Sp1-mediated signaling pathways. Carcinogenesis. 30, 356-365.

Peng Y., Shi J., Du X., Wang L., Klocker H., Mo L., Mo Z., and Zhang J. (2013). Prostaglandin E2 induces stromal cell-derived factor-1 expression in prostate stromal cells by activating protein kinase A and transcription factor Sp1. Int J Biochem Cell Biol. 45, 521-530.

Pompeia C., Freitas JJS., Kim JS., Zyngier SB., and Curi R. (2002). Arachidonic acid cytotoxicity in leukocytes: implications of oxidative stress and eicosanoid synthesis. Biol Cell. 94, 251-265.

Repesh LA., Fitzgerald TJ., and Furcht LT. (1982). Fibronectin involvement in granulation tissue and wound healing in rabbits. J Histochem Cytochem. 30, 351-358.

Ribeiro J., Pereira T., Amorim I., Caseiro AR., Lopes MA., Lima J., Gartner A., Santos JD., Bartolo PJ., Rodrigues JM., Mauricio AC., and Luis AL. (2014). Cell therapy with human MSCs isolated from the umbilical cord Wharton jelly associated to a PVA membrane in the treatment of chronic skin wounds. Int J Med Sci. 11, 979-987.

Sakayori N., Maekawa M., Numayama-Tsuruta K., Katura T., Moriya T., and Osumi N. (2011). Distinctive effects of arachidonic acid and docosahexaenoic acid on neural stem/progenitor cells. Genes Cells. 16, 778-790.

Sarbassov DD., Ali SM., Sengupta S., Sheen JH., Hsu PP., Bagley AF., Markhard AL., and Sabatini DM. (2006). Prolonged rapamycin treatment inhibits mTORC2 assembly and Akt/PKB. Mol Cell. 22, 159-168.

Sen B., Xie Z., Case N., Thompson WR., Uzer G., Styner M., and Rubin J. (2014). mTORC2 regulates mechanically induced cytoskeletal reorganization and lineage selection in marrow-derived mesenchymal stem cells. J Bone Miner Res. 29, 78-89.

Sivamani RK. (2014). Eicosanoids and Keratinocytes in Wound Healing. Adv Wound Care. 3, 476-481.

Smith AN., Muffley LA., Bell AN., Numhom S., and Hocking AM. (2012). Unsaturated fatty acids induce mesenchymal stem cells to increase secretion of angiogenic mediators. J Cell Physiol. 227, 3225-3233.

Strong AL., Semon JA., Strong TA., Santoke TT., Zhang SJ., McFerrin HE., Gimble JM., and Bunnell BA. (2012). Obesity-associated dysregulation of calpastatin and MMP-15 in adipose-

derived stromal cells results in their enhanced invasion. Stem Cells. 30, 2774-2783.

Sun XJ., Gao X., Zhou LY., Sun LJ., and Lu CL. (2013). PDGF-BB-induced MT1-MMP expression regulates proliferation and invasion of mesenchymal stem cells in 3-dimensional collagen via MEK/ERK1/2 and PI3K/AKT signaling. Cell Signal. 25, 1279-1287.

Tanaka K., Babic I., Nathanson D., Akhavan D., Guo DL., Gini B., Dang J., Zhu SJ., Yang HJ., De Jesus J., Amzajerdi AN., Zhang YN., Dibble CC., Dan HC., Rinkenbaugh A., Yong WH., Vinters HV., Gera JF., Cavenee WK., Cloughesy TF., Manning BD., Baldwin AS., and Mischel PS. (2011). Oncogenic EGFR signaling activates an mTORC2-NF-κB pathway that promotes chemotherapy resistance. Cancer Discov. 1, 524-538.

Tang JF., Wen Q., Sun J., Zhang WM., and Zhu HL. (2014a). Advances in the researches on the biological activities and inhibitors of phosphatidylinositol 3-kinase. Anticancer Agent Me. 14, 673-687.

Tang JM., Yuan J., Li Q., Wang JN., Kong X., Zheng F., Zhang L., Chen L., Guo LY., Huang YH., Yang JY., and Chen SY. (2012). Acetylcholine induces mesenchymal stem cell migration via Ca^{2+}/PKC/ERK1/2 signal pathway. J Cell Biochem. 113, 2704-2713.

Tang Z., Baykal AT., Gao H., Quezada HC., Zhang HY., Bereczki E., Serhatli M., Baykal B., Acioglu C., Wang S., Ioja E., Ji XY., Zhang Y., Guan ZZ., Winblad B., and Pei JJ. (2014b). mTor is a signaling hub in cell survival: a mass-spectrometry-based proteomics investigation. J Proteome Res. 13, 2433-2444.

Tomita T., Hosoda K., Fujikura J., Inagaki N., and Nakao K. (2014).The G-protein-coupled long-chain fatty acid receptor GPR40 and glucose metabolism. Front Endocrinol (Lausanne). 5, 152.

Treins C., Warne PH., Magnuson MA., Pende M., and Downward J. (2010). Rictor is a novel target of p70 S6 kinase-1. Oncogene. 29, 1003-1016.

Vaca P., Berna G., Araujo R., Carneiro EM., Bedoya FJ., Soria B., and Martin F. (2008). Nicotinamide induces differentiation of embryonic stem cells into insulin-secreting cells. Exp Cell Res. 314, 969-974.

Wang M., Yang Y., Yang DM., Luo F., Liang WJ., Guo SQ., and Xu JZ. (2009). The immunomodulatory activity of human umbilical cord blood-derived mesenchymal stem cells *in vitro*. Immunology. 126, 220-232.

Wang XS., Ge JF., Tredget EE., and Wu YJ. (2013). The mouse excisional wound splinting model, including applications for stem cell transplantation. Nat Protoc. 8, 302-309.

Yang SG., Ma YH., Liu Y., Que HP., Zhu CQ., and Liu SJ. (2012). Arachidonic acid: a bridge between traumatic brain injury and fracture healing. J Neurotrauma. 29, 2696-2705.

YauWWY., Rujitanaroj PO., Lam L., and Chew SY. (2012). Directing stem cell fate by controlled RNA interference. Biomaterials. 33, 2608-2628.

Yun SP., Lee SJ., Jung YH., and Han HJ. (2014a). Galectin-1

stimulates motility of human umbilical cord blood-derived mesenchymal stem cells by downregulation of smad2/3-dependent collagen 3/5 and upregulation of NF-κB-dependent fibronectin/laminin 5 expression. Cell Death Dis. 5, e1049.

Yun SP., Lee SJ., Oh SY., Jung YH., Ryu JM., Suh HN., Kim MO., Oh KB., and Han HJ. (2014b). Reactive oxygen species induce MMP12-dependent degradation of collagen 5 and fibronectin to promote the motility of human umbilical cord-derived mesenchymal stem cells. Br J Pharmacol. 171, 3283-3297.

Yusuf RZ., and Scadden DT. (2012). Fate through fat: lipid metabolism determines stem cell division outcome. Cell Metab. 16, 411-413.

Ziboh VA., and Chapkin RS.(1988). Metabolism and function of skin lipids. Prog Lipid Res. 27, 81-105.

국 문 초 록

아라키돈산에 의한 MT3-MMP 발현의 중간엽 줄기세포 이동 및 창상 치유능 증진 효과

서울대학교 대학원

수의학과 수의생명과학 전공

오 상 엽

지도교수 한 호 재

아라키돈산은 상처 부위로 많이 분비되지만, 그것이 줄기세포를 통해 상처 회복을 조절하는 방법에 대해선 많이 밝혀지지 않았다. 본 연구의 목적은 아라키돈산으로 자극한 인간 제대혈 유래 중간엽 줄기세포의 창상 회복 효과를 생체적으로, 그 분자적 기전을 시험관적으로 규명하는 것이다. 마우스 창상 모델에서 아라키돈산으로 전처리한 줄기세포 이식은 상처 메움, 재상피화, 그리고 혈관신생을 증진시켰다. 아라키돈산은

처리 후 24시간 째부터 줄기세포의 이동을 현저하게 촉진시켰고, 이는 GPR40 녹다운으로 억제되었다. 아라키돈산은 GPR40/PI3K 신호를 거쳐 mTORC2와 Akt^{ser473}을 활성화시켰고, 이는 비정형 PKCζ 자극을 유도하였다. 이어서 p38 MAPK와 전사인자 Sp1의 인산화를 유도하였고, MT3-MMP 의존적 FN 분해를 통해 줄기세포의 이동을 촉진시켰다. MT3-MMP 유전자를 억제한 줄기세포에 아라키돈산을 전처리하고 창상 부위에 이식하였더니, 세포이동장애로 회복이 촉진되지 않았다. 결론적으로 아라키돈산은 MT3-MMP 매개 FN 분해를 통해 줄기세포 이동을 유도하여 창상 회복을 증진시키고, 이는 GPR40 의존적 mTORC2 신호경로에 의한다.

주요어:아라키돈산, 중간엽 줄기세포, 창상 회복, 이동, MT3-MMP

학번 : 2013-21539